SCIENCE CHINA
Life Sciences

•COVER ARTICLE•

October 2020 Vol.63 No.10: 1429–1449
https://doi.org/10.1007/s11427-020-1631-9

Identification of mecciRNAs and their roles in the mitochondrial entry of proteins

Xu Liu[1], Xiaolin Wang[1], Jingxin Li[1], Shanshan Hu[2], Yuqi Deng[1], Hao Yin[1], Xichen Bao[3], Qiangfeng Cliff Zhang[4], Geng Wang[4], Baolong Wang[1], Qinghua Shi[1,5] & Ge Shan[1,5*]

[1]*Department of Clinical Laboratory, The First Affiliated Hospital of USTC, Hefei National Laboratory for Physical Sciences at Microscale, the CAS Key Laboratory of Innate Immunity and Chronic Disease, School of Basic Medical Sciences, Division of Life Science and Medicine, University of Science and Technology of China, Hefei 230027, China;*
[2]*Department of Neurosurgery, The First Affiliated Hospital of University of Science and Technology of China, Hefei 230001, China;*
[3]*Key Laboratory of Regenerative Biology of the Chinese Academy of Sciences, Joint School of Life Sciences, Guangzhou Medical University and Guangzhou Institutes of Biomedicine and Health, Chinese Academy of Sciences, Guangzhou 510530, China;*
[4]*MOE Key Laboratory of Bioinformatics, School of Life Sciences, Tsinghua University, Beijing 100084, China;*
[5]*CAS Center for Excellence in Molecular Cell Science, Shanghai Institute of Biochemistry and Cell Biology, Chinese Academy of Sciences, Shanghai 200031, China*

Received January 13, 2020; accepted January 19, 2020; published online January 21, 2020

Mammalian mitochondria have small genomes encoding very limited numbers of proteins. Over one thousand proteins and noncoding RNAs encoded by the nuclear genome must be imported from the cytosol into the mitochondria. Here, we report the identification of hundreds of circular RNAs (mecciRNAs) encoded by the mitochondrial genome. We provide both *in vitro* and *in vivo* evidence to show that mecciRNAs facilitate the mitochondrial entry of nuclear-encoded proteins by serving as molecular chaperones in the folding of imported proteins. Known components involved in mitochondrial protein and RNA importation, such as TOM40 and PNPASE, interact with mecciRNAs and regulate protein entry. The expression of mecciRNAs is regulated, and these transcripts are critical for the adaption of mitochondria to physiological conditions and diseases such as stresses and cancers by modulating mitochondrial protein importation. mecciRNAs and their associated physiological roles add categories and functions to the known eukaryotic circular RNAs and shed novel light on the communication between mitochondria and the nucleus.

mitochondria, circRNA, mecciRNA, mitochondrial protein import

Citation: Liu, X., Wang, X., Li, J., Hu, S., Deng, Y., Yin, H., Bao, X., Zhang, Q.C., Wang, G., Wang, B., et al. (2020). Identification of mecciRNAs and their roles in the mitochondrial entry of proteins. Sci China Life Sci 63, 1429–1449. https://doi.org/10.1007/s11427-020-1631-9

INTRODUCTION

Mammalian mitochondria harbor their own genome encoding 13 mitochondrial-specific proteins and multiple noncoding RNAs, such as 16S rRNA and some tRNAs (Anderson et al., 1981; Gustafsson et al., 2016). These proteins and RNAs represent a very small fraction of the mitochondrial contents, and more than one thousand proteins and an array of noncoding RNAs encoded by the nuclear genome are known to be transported into mammalian mitochondria to sustain the homeostasis and duplication of these cell organelles (Harbauer et al., 2014).

Over one thousand mitochondrial proteins encoded by the nuclear genome are imported into mitochondria through the outer membrane TOM40 complex, and some of them are transported with the assistance of cytosolic chaperones of the

*Corresponding author (email: shange@ustc.edu.cn)

heat-shock family proteins (Deshaies et al., 1988; Young et al., 2003). Some nuclear-encoded noncoding RNAs, such as MRP RNA (RMRP), 5S rRNA, and certain tRNAs, are also imported into mitochondria, although the mitochondrial RNA importation mechanism is much less well understood (Smirnov et al., 2010; Wang et al., 2010). It has been shown that the polynucleotide phosphorylase (PNPASE) PNPT1, residing in the mitochondrial intermembrane space, plays an unanticipated role in mitochondrial RNA importation (Cheng et al., 2018; Wang et al., 2010).

Essentially all mitochondrial functions rely on the import of proteins and RNAs, and cells must manage their import according to different physiological conditions (Harbauer et al., 2014; Quirós et al., 2015; Smirnov et al., 2010; Sokol et al., 2014). When mitochondrial functions are compromised, nuclear responses such as the mtUPR (mitochondrial unfolded protein response), UPRam (unfolded protein response activated by mistargeting of proteins), and mPOS (mitochondrial precursor over-accumulation stress) are triggered to induce the expression of mitochondrial chaperones and the degradation of unimported proteins and reduce mRNA translation in the cytosol(Boos et al., 2019; Scheibye-Knudsen et al., 2015; Topf et al., 2016; Wrobel et al., 2015). Whether and how the mitochondria themselves cope with dynamic cellular conditions by regulating protein importation remain much less studied (Moye-Rowley, 2003; Weidberg and Amon, 2018).

In an effort to reveal novel RNAs in mitochondria, we identified hundreds of circular RNAs (circRNAs) encoded by the mitochondrial genome (mecciRNAs) from both human and murine cells. Recent years have witnessed the identification of thousands of circRNAs encoded by the nuclear genome, and some of these circRNAs function as ceRNAs (microRNA sponges), protein binding partners, and transcriptional regulators (Chen, 2016; Chen et al., 2015; Li et al., 2015; Memczak et al., 2013). Here, we provide several lines of evidence to show that some of the mitochondria-encoded circRNAs can facilitate the mitochondrial entry of proteins encoded by the nuclear genome. The mitochondria modulate the amount of specific proteins imported into these organelles through mecciRNAs to adjust to physiological conditions.

RESULTS

Identification of mitochondria-encoded circRNAs

We sequenced RNAs from isolated mitochondria and analyzed the RNA-sequencing (RNA-seq) data with pipelines for identifying circRNAs encoded by either the nuclear genome or the mitochondrial genome (Figure 1A). In four cell lines and tissues, 248 and 268 high-confidence (with ≥2 junction reads) mitochondria-encoded circRNAs (mecciRNAs) were identified in humans and mice, respectively (Figure 1B; Figure S1A in Supporting Information). To expand the search, we also sequenced mitochondrial RNAs from adult male zebrafish (*Danio rerio*), and 139 mecciRNAs were identified (Figure 1B; Figure S1A in Supporting Information). Thus, hundreds of mecciRNAs are present in vertebrates (Table S1 in Supporting Information). Bioinformatics analysis revealed that some circRNAs encoded by the nuclear genome (g-circRNAs) were also present in the isolated mitochondria, although at significantly lower concentrations (RPM) than the mecciRNAs (Figure 1B). The mecciRNAs and g-circRNAs shared similar AG/GT junction motifs (Figure 1C; Figure S1B in Supporting Information). Consistent with previous studies (Gustafsson et al., 2016), no linear splicing events were identified in the mitochondrial transcripts. mecciRNAs were encoded by both the light and heavy strands of the mtDNA, and the heavy strand of mtDNA encoded the majority of mecciRNAs (224/248 in humans, 201/268 in mice, and 103/139 in zebrafish) (Table S1 in Supporting Information); the majority of mitochondrial mRNAs (12/13), tRNAs (14/22), and the 2 rRNAs, are also encoded by the heavy strand. Other features of mecciRNAs such as the size distribution of mecciRNAs were also analyzed (Figure S1C in Supporting Information).

We then verified some of these mecciRNAs via Northern blotting and RT-PCR (Figure 1D; Figure S2A–E in Supporting Information). To exclude potential misidentification of junction sites due to differences in the annotated genome and genome of cultured cells, nuclear DNA and mitochondrial DNA from HeLa cells were re-sequenced, and no DNA reads matching the junction sequences of human mecciRNAs were identified (Figure S3A in Supporting Information). In previously published RNA-seq data from cells without mitochondria (rho0 MEF cells), no mecciRNAs were identified, whereas mecciRNAs were found in wild type MEF cells (Shimada et al., 2018) (Figure S3B in Supporting Information). Interestingly, considering the small size of the mitochondrial genome, mecciRNAs were relatively enriched in nascent circRNAs detected from HeLa cells (Bao et al., 2018) (Figure S3C in Supporting Information). Another finding that might be related to the biogenesis of mecciRNAs was that the 4 nt (allowing a 1 nt mismatch) upstream of the 5′ junction site was repeated at the upstream of the 3′ junction site in approximately 40%–50% of mecciRNAs; the 4 nt (allowing 1 nt mismatch) downstream of the 3′ junction site was repeated at the downstream of the 5′ junction site in approximately 40%–50% of mecciRNAs (Figure S3D in Supporting Information). Additionally, thousands of g-circRNAs, but no mecciRNAs, were identified in the RNA-seq of nuclear RNA samples from isolated nuclei of human HeLa and HEK293T cells as well as murine N2a and 3T3 cells.

Furthermore, mecciRNAs only accounted for a very small

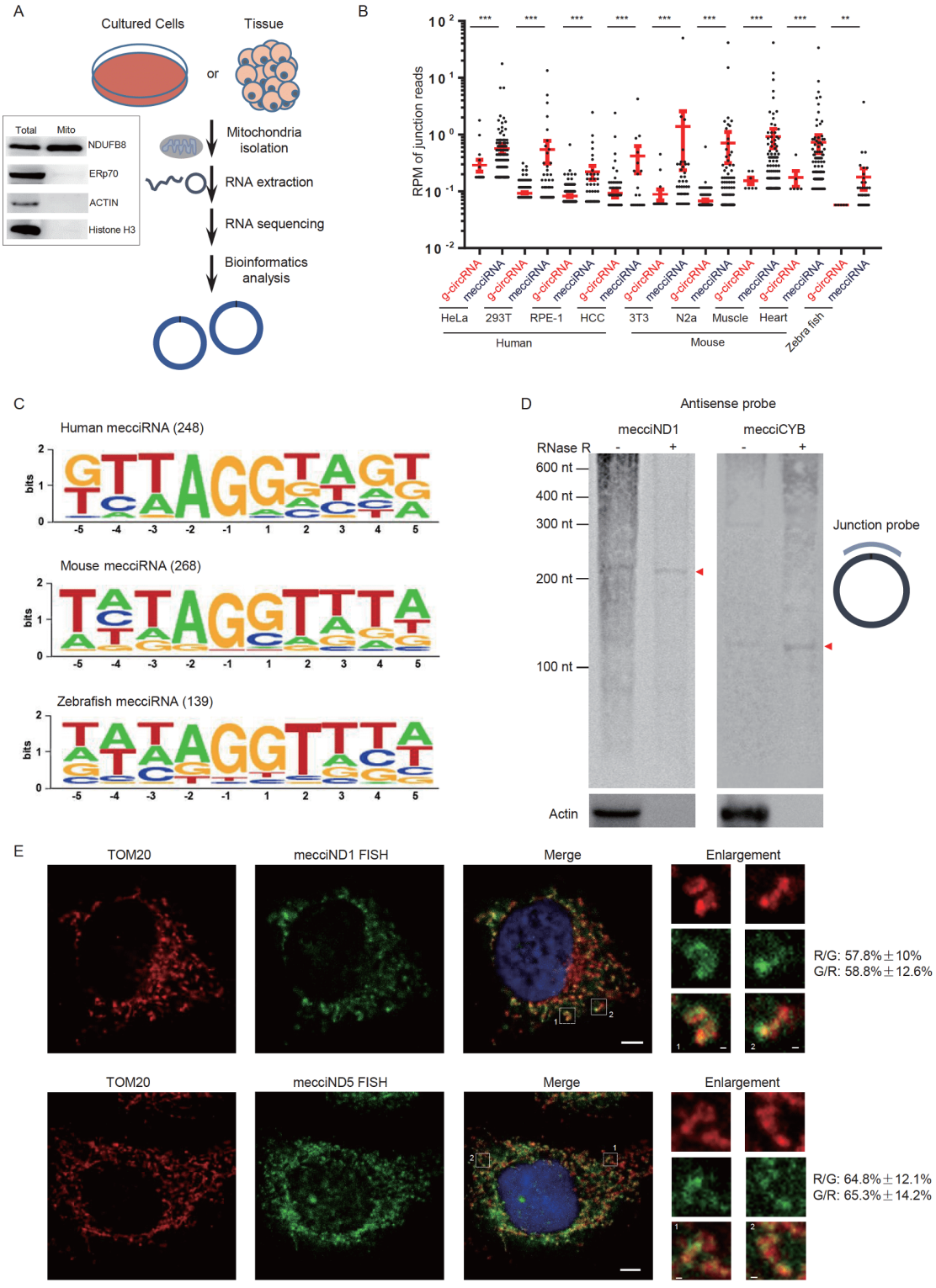

Figure 1 Identification and characterization of mecciRNAs. A, Experimental procedures for mitochondrial RNA sequencing to identify mecciRNAs; Western blots showing the quality of the purified mitochondria are presented; ERp70, ER marker; Histone H3, nuclear marker; ACTIN, cytosolic marker; NDUFB8, a mitochondrial inner membrane protein. B, g-circRNAs and mecciRNAs (reads ≥2) identified from the sequencing data of mitochondrial (mito) RNAs in human and murine cells and tissues; HCC, hepatocellular carcinoma. C, Junction motif of human, mouse and zebrafish (adult male) mecciRNAs. D, Northern blots of mecciRNAs. RNase R-treated (+) and untreated (–) total RNAs from HeLa cells were examined; the position of the probe is indicated; actin mRNA served as a linear control. E, Confocal images in single z-sections of TOM20 immunofluorescence (IF) together with FISH of mecciND1 or mecciND5. Boxed areas are enlarged. The colocalization between mecciND1 or mecciND5 (G, green) and TOM20 (R, red) is shown (n=20 randomly selected areas). R/G, proportion of red signal to green signal colocalization; G/R, proportion of green signal to red signal colocalization. Scale bar, 5 μm and 500 nm (enlarged areas) in E; error bars represent standard error of the mean in B; $^{**}P<0.01$; $^{***}P<0.001$ by two-tailed Mann-Whitney U test.

portion of all circRNAs in the cytoplasm, as g-circRNAs were much more prevalent in molecule numbers than mecciRNAs (Figure S4A in Supporting Information). In contrast to mitochondrion-encoded mRNAs, mecciRNAs were also present outside of the mitochondria (Figure S4B in Supporting Information). We then examined two mecciRNAs encoded by the mitochondrial gene ND1 (mecciND1) and ND5 (mecciND5) in detail. RNA fluorescence *in situ* hybridization (FISH) combined with immunofluorescence (IF) of TOM20 (a mitochondrial outer membrane protein) revealed that both the FISH signals of mecciND1 and mecciND5 partially overlapped with the TOM20 IF signals (Figure 1E). Some portion of mecciND1 and mecciND5 signals did not overlap with the mitochondrial TOM20 signals, indicating that these mecciRNAs were also present outside of the mitochondria and in the cytosol (Figure 1E). For comparison, the FISH signals of the ND1 mRNAs largely colocalized with the TOM20 IF signals (Figure S4C in Supporting Information).

Interaction between mecciND1 and RPA proteins

We decided to investigate the potential functions of mecciRNAs using mecciND1. Pulldown of mecciND1 with an antisense probe was performed, and two proteins, RPA70 and RPA32, were identified after being co-pulled down with this circRNA (Figure 2A; Figure S5A, Table S2 in Supporting Information). RPA70 and RPA32 are subunits of the replication protein A complex that binds to single-stranded DNA. The interaction between mecciND1 and RPA70 and RPA32 proteins was then confirmed via RNA pulldown followed by Western blotting and protein immunoprecipitation followed by RNA detection (RNA-IP, or RIP) (Figure 2B–D; Figure S5B in Supporting Information). We also noticed that RPA proteins (RPA32 was examined) might be relatively specific in binding to mecciND1, compared to the other three highly expressed mecciRNAs (Figure S5C in Supporting Information). FISH analysis of mecciND1 along with IF of RPA proteins and TOM20 showed that over half of the mecciND1 signals overlapped with mitochondria and cytoplasmic RPA proteins (Figure S5D in Supporting Information).

We next examined the localization of TOM40, RPA32, and mecciND1 in greater detail via super-resolution N-SIM (Figure 2E; Figure S5E in Supporting Information). At the resolution of SIM, we could differentiate whether the fluorescent signals came from inside or outside of the mitochondrion (the TOM40-enclosed space). We observed that some RPA32 and mecciND1 signals localized inside of the TOM40 enclosed space, and a portion of RPA32 and mecciND1 signals exhibited colocalization around or inside the TOM40 signals (Figure 2E; Figure S5E in Supporting Information). Some fraction of RPA32 and mecciND1 was also localized outside the mitochondria (Figure 2E; Figure S5E in Supporting Information).

Interaction between mecciND5 and hnRNPA proteins

We next investigated whether another mecciRNA, mecciND5, could interact with specific proteins. Antisense probe pulldown of mecciND5 revealed that three proteins: hnRNPA1, hnRNPA2B1, and hnRNPA3 were co-pulled down (Figure 2F; Figure S6A, Table S2 in Supporting Information). RNA pulldown of mecciND5 followed by Western blotting detected hnRNPA1, hnRNPA2B1, and hnRNPA3 (collectively hnRNPA proteins) (Figure 2G). The heterogeneous nuclear ribonucleoproteins A1, A2B1, and A3 share high homology, and hnRNPA1 was the predominant protein among the hnRNPA proteins interacting with mecciND5 (Figure 2F and G; Figure S6B in Supporting Information). RNA-IP with antibodies against hnRNPA1 showed enrichment of mecciND5 (Figure 2H). hnRNPA1 bound mecciND1 and the other three highly expressed mecciRNAs, although its binding to mecciND5 was relatively strong (Figure S6B in Supporting Information). IF of hnRNPA proteins and TOM20 revealed that more than half of the cytoplasmic hnRNPA proteins colocalized with TOM20 (Figure S6C in Supporting Information). More than half of the cytoplasmic hnRNPA IF signals also colocalized with cytoplasmic mecciND5 signals (Figure S6C in Supporting Information). Through super-resolution N-SIM, we found that hnRNPA1 and mecciND5 had localizations inside the TOM40-enclosed space, and hnRNPA1 and mecciND5 had colocalizations around TOM40 signals (Figure 2I; Figure S6D in Supporting Information). Some fraction of hnRNPA1 and mecciND5 also localized outside the mitochondria (Figure 2I; Figure S6D in Supporting Information).

Mitochondrial RPA levels are regulated by mecciND1

Interestingly, knockdown of mecciND1 with siRNAs decreased RPA70 and RPA32 protein levels in mitochondria, although the total levels of both proteins were not or less affected (Figure 3A; Figure S7A in Supporting Information). In another attempt to interfere with mecciND1, we applied antisense morpholino oligos (AMO) against mecciND1 (Figure S7B in Supporting Information). Surprisingly, mitochondrial RPA protein (especially RPA32) levels were increased after mecciND1-AMO transfection (Figure S7B in Supporting Information). We found that the whole-cell levels of mecciND1 were not altered, but cytosolic mecciND1 levels were increased (Figure S7B in Supporting Information). This result suggested that mecciND1-AMO somehow held mecciND1 in the cytosol, and the higher cytosolic mecciND1 levels resulted in more RPA32 importation into

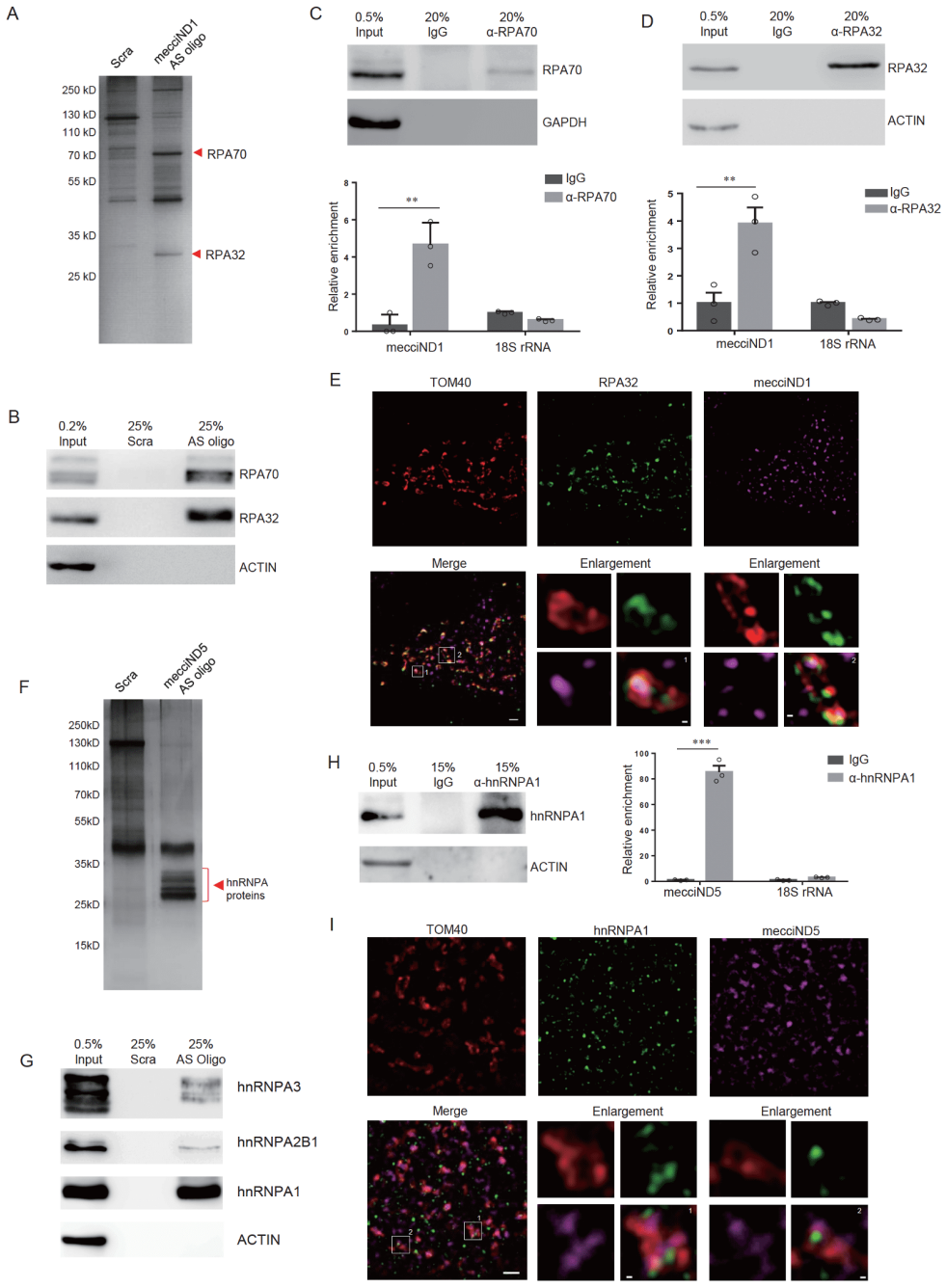

Figure 2 mecciND1 interacts with RPA70 & RPA32, and mecciND5 interacts with hnRNPA proteins. A, Pulldown of MecciND1 with biotin-labelled antisense oligos (AS oligos) in HeLa cells. Proteins that were co-pulled down with mecciND1 were subjected to silver staining; red triangles indicate the bands identified as RPA70 and RPA32 by mass spectrometry. Scra, oligos with scrambled sequences. B, RPA70 and RPA32 co-pulled down with mecciND1 were verified by Western blotting; ACTIN, negative control. C, RNA immunoprecipitation (RIP) against RPA70 (α-RPA70) with whole-cell HeLa cell lysates. Successful IP of the protein was detected by Western blotting; GAPDH, negative control. RNAs from RIP were quantified by real-time qPCR; 18S rRNA, negative control. D, RNA immunoprecipitation (RIP) against RPA32 (α-RPA32) with whole-cell HeLa cell lysates. Successful IP of the protein was detected by Western blotting; GAPDH, negative control. RNAs from RIP were quantified by real-time qPCR; 18S rRNA, negative control. E, Representative structured illumination microscopy images (N-SIM) from single z-sections of RPA32 immunofluorescence (IF) together with TOM40 as well as FISH of mecciND1 in fixed HeLa cells. Boxed areas are enlarged; scale bar, 2 μm and 200 nm (enlarged areas). F, Pulldown of mecciND5 with biotin-labelled antisense oligo in HeLa cells (experimental details were slightly different from pulldown of mecciND1 shown in A, see Methods). Proteins that were co-pulled down with mecciND5 were subjected to silver staining; red triangles indicate the bands identified as hnRNPA1, hnRNPA2B1 and hnRNPA3 by mass spectrometry. Scra, oligos with scrambled sequences. G, hnRNPA1, hnRNPA2B1, and hnRNPA3 co-pulled down with mecciND5 were verified by Western blotting; ACTIN, negative control. H, RNA immunoprecipitation (RIP) against hnRNPA1 (α-hnRNPA1) with whole-cell lysate of HeLa cells. Successful IP of the protein was detected by Western blotting; ACTIN, negative control. RNAs from RIP were quantified by real-time qPCR; Actin mRNA, negative control. I, Representative structured illumination microscopy (N-SIM) images in single z-sections of hnRNPA1 and TOM40 immunofluorescence (IF) as well as FISH of mecciND5 in fixed HeLa cells. Scale bar, 2 μm and 200 nm (boxed areas are enlarged). In C, D, and H, the error bars represent standard error of the mean; n=3 independent experiments; $^{**}P<0.01$, $^{***}P<0.001$, Student's t-test.

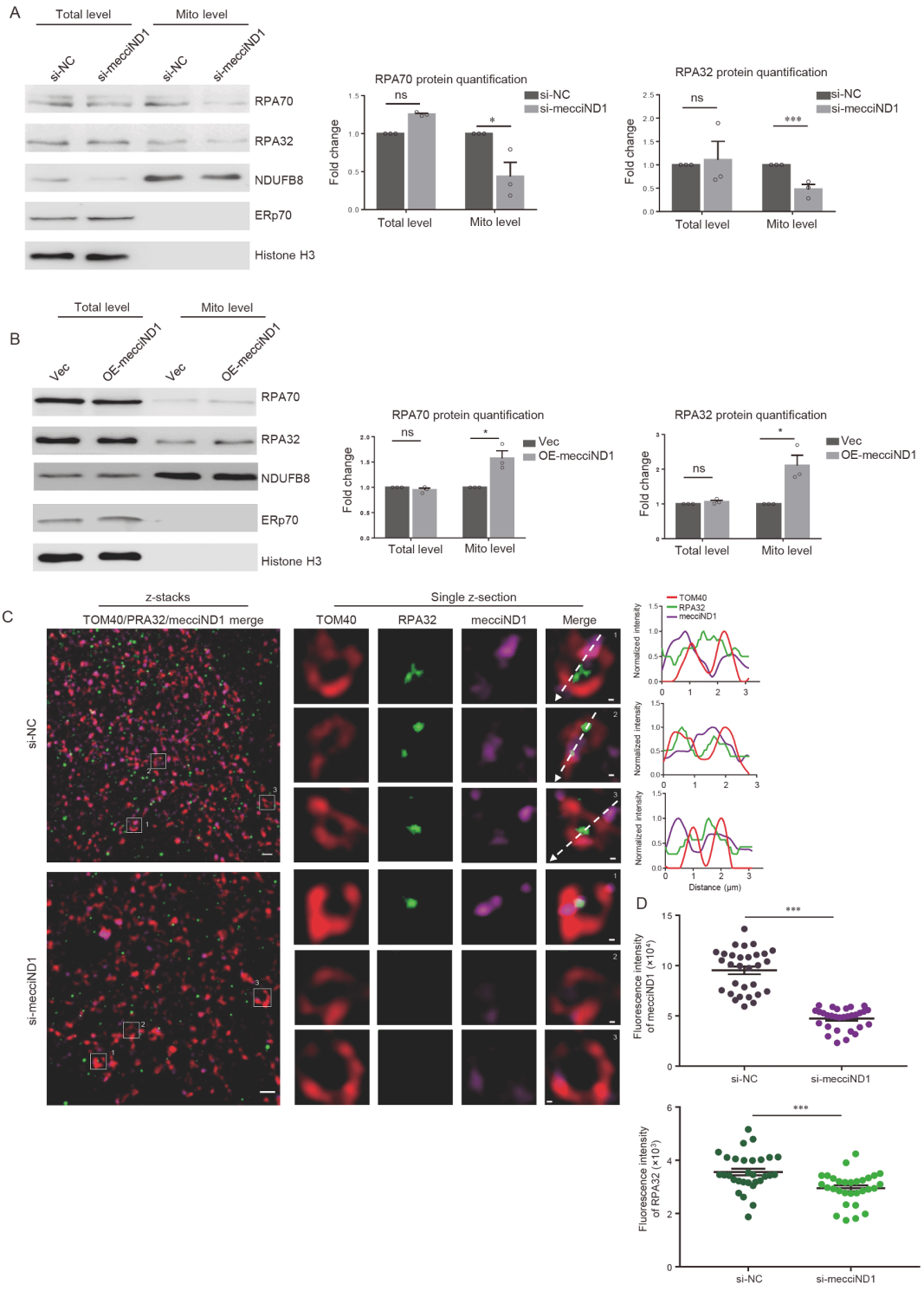

Figure 3 mecciND1 regulates mitochondrial RPA levels. A, Mitochondrial RPA70 and RPA32 protein levels were decreased after knockdown of mecciND1 via siRNA in 293T cells. Western blots of proteins from whole cells (total level) and mitochondria (mito level) were examined; si-NC, siRNA with scrambled sequences; NDUFB8 served as a loading control for mitochondrial protein levels; ERp70, an endoplasmic reticulum marker, served as a loading control for whole-cell protein levels; Histone H3, a nuclear marker. The results of the quantification of RPA proteins are shown. B, Mitochondrial RPA70 and RPA32 protein levels were increased under mecciND1 overexpression in 293T cells. C, Representative structured illumination microscopy images in z-stacks (3D N-SIM) of RPA32 and TOM40 immunofluorescence (IF) as well as FISH of mecciND1 in fixed RPE-1 cells transfected with siRNA (si-NC or si-mecciND1). Plot profiles of representative images of TOM40 and RPA32 IF signals as well as FISH of mecciND1 are shown for si-NC group. Images of single z-sections of the boxed areas are enlarged. Scale bar, 2 μm and 200 nm (enlarged areas). D, The results of quantification of the fluorescence signals of mecciND1 and RPA32 via N-SIM are shown; areas representing single mitochondria were selected, and fluorescence signals overlapping the TOM40 signal or inside the TOM40-enclosed space were quantified; n=30 randomly chosen areas. In A, B, and D, error bars represent standard error of the mean; in A and B, n=3 independent experiments; ns, not significant; *P<0.05, **P<0.01, ***P<0.001 by Student's t-test.

mitochondria. We next found that mecciND1 could be overexpressed with a nuclear-transfected plasmid (Figure S7C in Supporting Information). Overexpression of mecciND1 with nuclear plasmid increased RPA70 and RPA32 protein levels in mitochondria, and the total levels of both proteins were again not significantly changed (Figure 3B). Neither mecciND1 knockdown nor overexpression affected mRNA levels of RPA70 and RPA32 (Figure S7D in Supporting Information). When the RPA32 signals inside TOM40-enclosed space were examined via N-SIM, they were found to be significantly decreased in the mecciND1 knockdown cells compared to those in control cells; nuclear levels of RPA32 signals were not altered (Figure 3C and D; Figure S7E–G in Supporting Information).

Mitochondrial hnRNPA levels are regulated by mecciND5

Knockdown of mecciND5 with siRNAs decreased hnRNPA protein levels in mitochondria, but the total levels of all three hnRNPA proteins and mRNAs were much less affected (Figure 4A; Figure S8A in Supporting Information). Mitochondrial hnRNPA protein levels were found to be increased after mecciND5-AMO transfection (Figure S8B in Supporting Information). The whole-cell levels of mecciND5 were unchanged, but cytosolic mecciND5 levels were increased (Figure S8B in Supporting Information). Overexpression of mecciND5 with a nuclear expressed plasmid increased hnRNPA1 and hnRNPA2B1 protein levels in mitochondria, while the whole-cell levels of all hnRNPA proteins and mRNAs were unchanged (Figure 4B; Figure S8C and D in Supporting Information). When examined via N-SIM, the hnRNPA1 signals inside the TOM40-enclosed space were significantly decreased in the mecciND5 knockdown cells compared to those in control cells; nuclear levels of hnRNPA1 signals were not altered (Figure 4C and D; Figure S8E–G in Supporting Information).

Taken together, the results indicated that the cellular levels of both mecciND1 and mecciND5 were positively correlated with levels of their corresponding protein partners inside mitochondria, and these data suggested the possibility that both mecciRNAs promoted mitochondrial importation of specific proteins. The abundance of these RNAs meant that it was reasonable for them to play this role, as there were ~52–109 molecules of mecciND1 and ~118–330 molecules of mecciND5 in each cell in the four cell lines that we examined (Figure S9A in Supporting Information).

mecciRNAs promote mitochondrial importation in *in vitro* assays

We then performed a series of assays with purified mitochondria and *in vitro* transcribed linear and circular RNA (Wesselhoeft et al., 2018) (Figure S9B and C in Supporting Information). Using an RNA import assay, we found that extra-mitochondrial mecciND1 and mecciND5, but not the g-circRNA circSRSF, could be imported into mitochondria, whereas all of their linear forms could not enter mitochondria (Figure 5A). When mecciND1 was added together with RPA32 mRNA in the rabbit reticulocyte translational system (to examine the co-translational effect of mecciRNA), mecciND1 increased the mitochondrial importation of the *in vitro*-translated RPA32 protein (Figure 5B; Figure S9D in Supporting Information). Similarly, co-translationally added mecciND5 also increased the mitochondrial importation of *in vitro*-translated hnRNPA1 (Figure 5C; Figure S9E in Supporting Information). We noticed that the addition of circRNAs co-translationally lowered the yield of protein, although more proteins were imported into mitochondria in the presence of mecciRNAs (Figure 5B and C). Interestingly, when added after the translation of the RPA32 protein (post-translation), mecciND1 still increased the mitochondrial importation of the RPA32 protein, although with a much weaker effect compared to the co-translational setup (Figure 5B and D). MecciND5 had no effect on the mitochondrial importation of the hnRNPA1 protein when added post-translationally, and actually, there was little hnRNPA1 getting imported into the mitochondria in the post-translational setup, with or without mecciND5 (Figure 5E). These data suggested that mecciRNAs might promote the formation of protein structures that favor the mitochondrial importation of newly synthesized polypeptides, whereas once the proteins had adopted certain structure, mecciRNAs added post-translationally would have less effect. We also examined whether mecciND1 or mecciND5 was specific in the co-translational promoting of mitochondrial importation of its protein cargo. We found that mecciND5 promoted RPA32 protein importation, but with a weaker enhancing effect than mecciND1, and mecciND1 did not promote the mitochondrial importation of hnRNPA1 (Figure S9F and G in Supporting Information). MecciND1 and mecciND5 imported into mitochondria could also be exported into the buffer in the *in vitro* assays (Figure S9H in Supporting Information). This result was consistent with the cellular localization of mecciRNAs in both the mitochondria and cytosol; mecciRNAs might shuttle between mitochondria and cytosol.

mecciRNAs interact with known components of mitochondrial importation

It would be reasonable to propose that mecciRNAs such as mecciND1 and mecciND5 interact with complexes such as TOM40 to facilitate protein entry into mitochondria. RNA-IP targeting TOM40 complex proteins TOM40 and TOM20 (both FLAG tagged) was performed, and mecciRNAs including mecciND1 and mecciND5 were found to interact

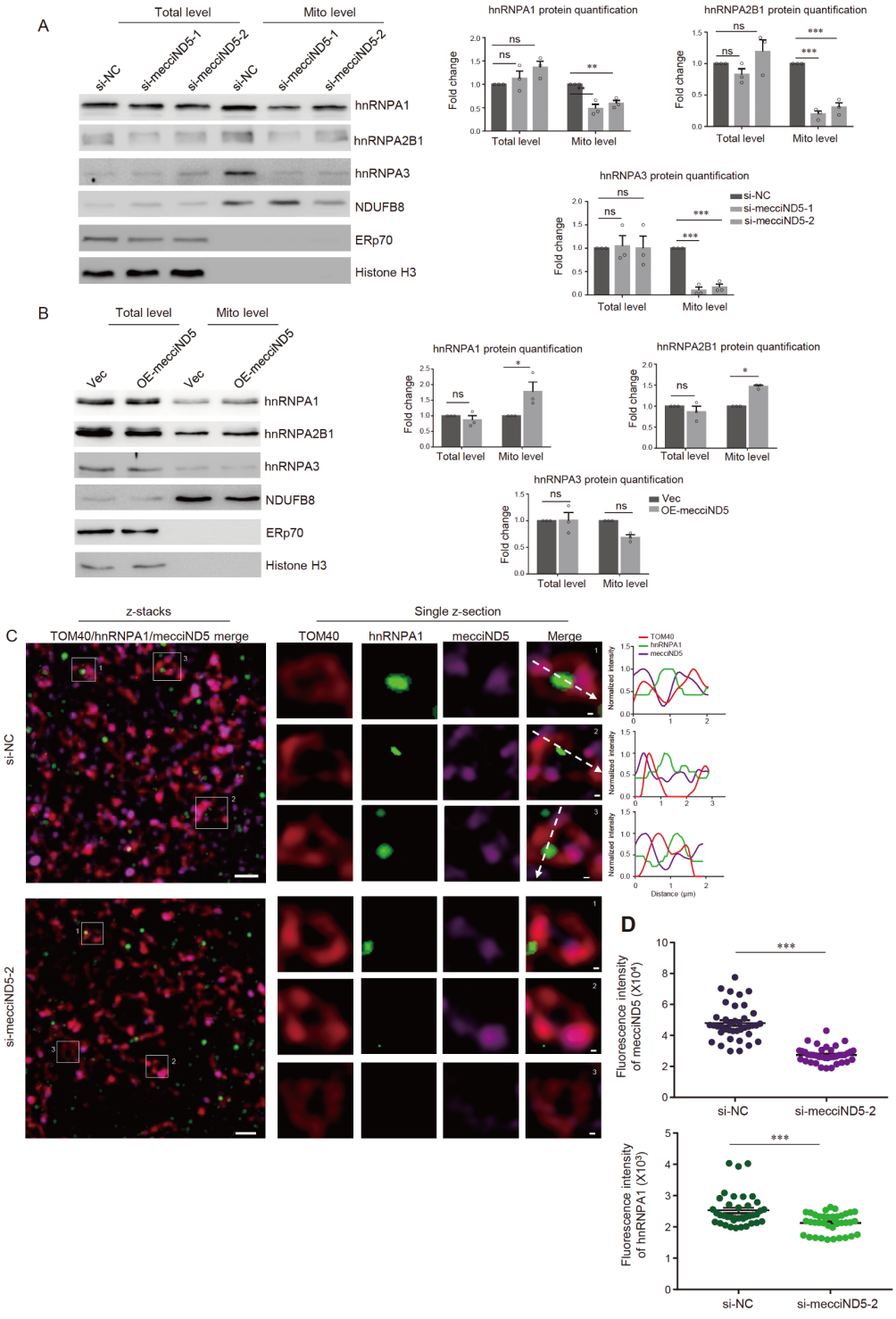

Figure 4 mecciND5 regulates mitochondrial hnRNPA levels. A, Mitochondrial hnRNPA1, hnRNPA2B1, and hnRNPA3 protein levels were decreased after knockdown of mecciND5 with siRNAs in 293T cells. Western blots of proteins from whole cells (total level) and mitochondria (mito level) are shown; si-NC, siRNA with scrambled sequences; NDUFB8 served as a loading control for mitochondrial protein levels; ERp70, an endoplasmic reticulum marker, served as a loading control for whole-cell protein levels; Histone H3, a nuclear marker. The results of the quantification of hnRNPA proteins are shown. B, Mitochondrial hnRNPA1, hnRNPA2B1, and hnRNPA3 protein levels were increased under mecciND5 overexpression in 293T cells. C, Representative structured illumination microscopy images in z-stacks (3D N-SIM) of hnRNPA1 and TOM40 immunofluorescence (IF) as well as FISH of mecciND5 in fixed RPE-1 cells transfected with siRNA (si-NC or si-mecciND5).Plot profiles of representative images of TOM40 and hnRNPA1 IF signals as well as FISH of mecciND5 are shown for si-NC group. Single z-section images of boxed areas are enlarged. Scale bar, 2 μm and 200 nm (enlarged areas). D, The results of the quantification of the fluorescence signals of mecciND5 and hnRNPA1 via N-SIM are shown; areas representing single mitochondria were selected, and fluorescence signals that overlapped with the TOM40 signal or were inside the TOM40-enclosed space were quantified; n=39 randomly chosen areas.In A, B, and D, error bars represent standard error of the mean; in A and B, n=3 independent experiments; ns, not significant; *P<0.05; **P<0.01; ***P<0.001, Student's t-test.

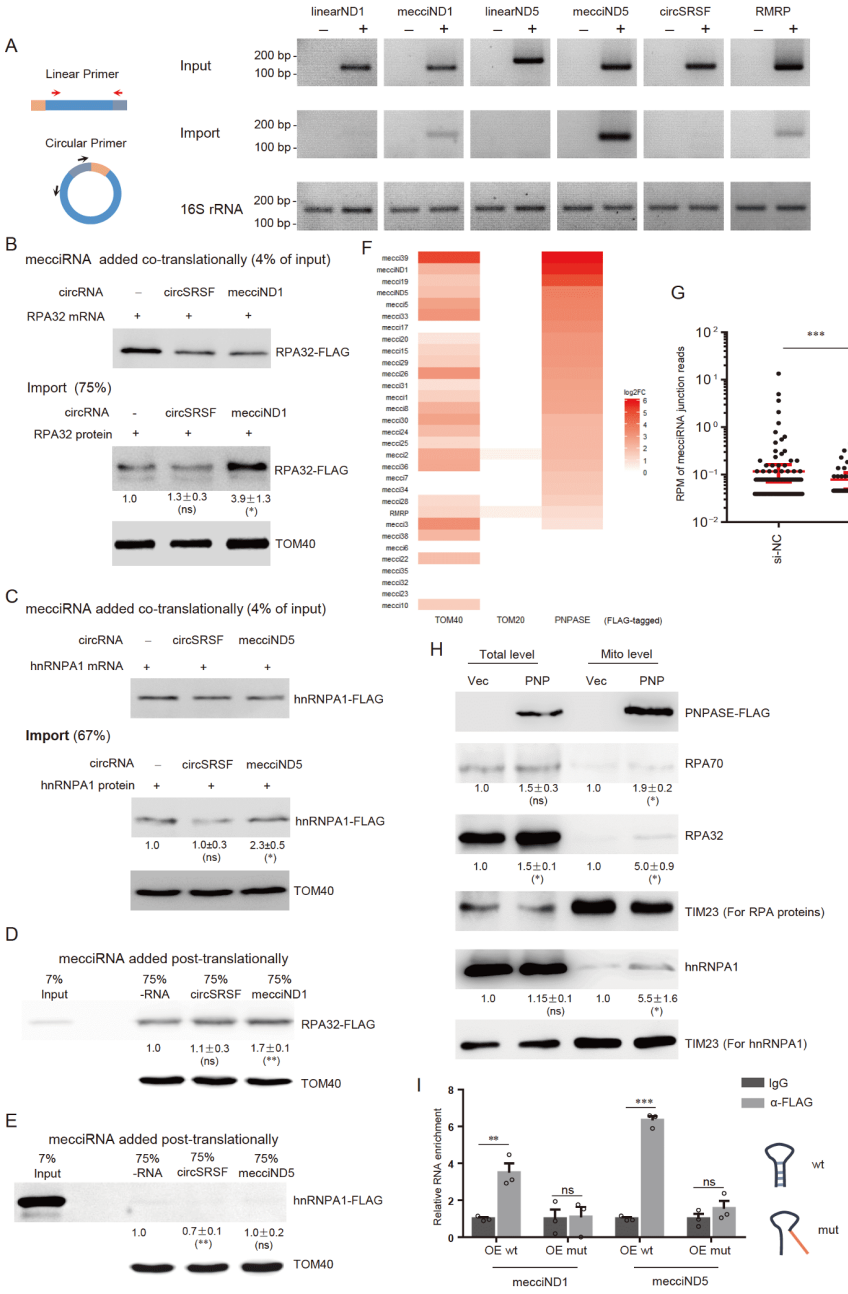

Figure 5 mecciRNAs promote mitochondrial importation in *in vitro* assays and interact with known components of mitochondrial importation. A, Semi-quantitative RT-PCR of *in vitro* RNA import assays. The linear RNA and the counterpart mecciRNA share the same sequences. circSRSF, a g-circRNA control; RMRP, a nuclear-encoded linear RNA that can be imported into mitochondria, positive control; 16S rRNA, mitochondrion-encoded rRNA, loading control and a marker for mitochondrial integrity. B, mecciND1 added with RPA32 mRNA in the rabbit reticulocyte translational system (co-translation) and the mitochondrial importation of the *in vitro*-translated RPA32-FLAG protein. Upper, translation products of RPA32-FLAG protein (Input); lower, RPA32-FLAG protein imported into mitochondria. C, mecciND5 added together with hnRNPA1 mRNA in the rabbit reticulocyte translational system (co-translation) and the mitochondrial importation of *in vitro*-translated hnRNPA1-FLAG protein. Upper, translation products of hnRNPA1-FLAG protein (Input); lower, hnRNPA1-FLAG protein imported into mitochondria. D, Mitochondrial importation of the *in vitro*-translated RPA32-FLAG protein with mecciND1 added post-translationally. E, Mitochondrial importation of the *in vitro*-translated hnRNPA1-FLAG protein, mecciND5 added post-translationally. For B–E, circSRSF, a g-circRNA control; TOM40, mitochondrial outer membrane protein, a loading control; the relative importation efficacy of the protein was calculated. F, RNA immunoprecipitation (RIP) against FLAG-tagged TOM40, TOM20 and PNPASE with lysates of transfected 293T cells. The levels of mecciRNA enrichment were examined by real-time qPCR, and the fold changes (log2FC) compared to the IgG control were then converted into a heatmap. G, Mitochondrial mecciRNA levels from mitochondrial RNA-seq data after knockdown of PNPASE. Error bars, standard error of the mean (SEM); ***P<0.001 by the two-tailed Mann-Whitney U test. H, Mitochondrial RPA protein levels and hnRNPA1 protein levels under overexpression of the PNPASE protein in 293T cells; Vec, vector control; PNP, PNPASE overexpression. TIM23, a mitochondrial inner membrane protein, loading control.I, RNA immunoprecipitation (RIP) against FLAG-tagged PNPASE with a cell lysate (293T cells) co-transfected with wild-type (wt) or stem-loop-mutated (mut) mecciND1/mecciND5. For B–E and H, the results of the quantification of protein levels were normalized to mitochondrial loading controls (TOM40 or TIM23), and the relative levels were the ratios to the corresponding control. n=3 independent experiments; data are the mean±SEM; ns, not significant; *P<0.05; **P<0.01; Student's t-test. In I, error bars, SEM; ns, not significant; **P<0.01; ***P<0.001 by Student's t-test.

with TOM40 (the channel-forming protein of the TOM40 complex), but not TOM20 (the major import receptor for mitochondrial signal peptide sequences) (Harbauer et al., 2014; Wiedemann and Pfanner, 2017) (Figure 5F; Figure S10A and B in Supporting Information). PNPASE, a major mitochondrial RNA importation factor, was also examined, and most of the mecciRNAs examined interacted with PNPASE (Figure 5F; Figure S10A and B in Supporting Information). Knockdown of PNPASE led to decreased mitochondrial mecciRNA levels (Figure 5G; Figure S10C in Supporting Information). Overexpression of PNPASE increased mitochondrial RPA and hnRNPA1 protein levels as well as mecciND1 and mecciND5 levels (Figure 5H; Figure S10D in Supporting Information). A small stem-loop structure in RNAs can facilitate mitochondrial RNA importation through PNPASE (Wang et al., 2010). There was a predicted small stem-loop in both mecciND1 and mecciND5, and data from a published icSHAPE assay for detecting *in vivo* RNA secondary structure demonstrated that the stem-loop structures predicted in mecciND1 and mecciND5 might be actual structures (Sun et al., 2019); deletion of the stem-loops abolished the interaction between PNPASE and the two mecciRNAs (Figure 5I; Figures S10E and S11).

Dynamic expression of mecciND1 and its association with cellular physiology

Under both UV and hydrogen peroxide treatments, increased mecciND1 levels were observed and showed a positive correlation with increased mitochondrial RPA70 and RPA32 protein levels (Figure 6A and B). The total protein levels of RPA32 and RPA70 were not changed under UV treatment, and their mitochondrial levels increased about two-fold (Figure 6A). Both RPA proteins showed about two-fold increase in total levels and more dramatic increase in mitochondrial levels under hydrogen peroxide treatment (Figure 6B). Using immunogold staining, we observed that levels of RPA32 in the mitochondria increased upon hydrogen peroxide treatment (Figure 6C). The levels of mecciND1 also increased upon cellular stresses resulting from hypoxia and tunicamycin treatments (Herst et al., 2017) (Figure S12A and B in Supporting Information). UV, hydrogen peroxide, hypoxia, and tunicamycin are known to induce DNA damage, and thus, trigger DNA repair in mitochondria (Herst et al., 2017; Van Houten et al., 2006). It is believed that mtDNA is more susceptible to oxidative damage than nuclear DNA under regular or stressed physiological conditions because mtDNA is located in proximity to the ROS-generating respiratory chain (Herst et al., 2017; Van Houten et al., 2006). RPA70 and RPA32 are well known to form complexes and to be essential in the repair and duplication of genomic DNA by binding to single-stranded DNA (Zou et al., 2006). Knockdown of RPA70 and RPA32 decreased the copy number of mitochondrial DNA (mtDNA) (Figure 6D), indicating that RPA proteins are also involved in the duplication of mtDNA. Consistent with the observed changes in the mitochondrial levels of RPA proteins, mtDNA copy numbers were decreased upon mecciND1 knockdown and increased under mecciND1 overexpression (Figure 6E).

Mitochondria are closely related to cancers (Vyas et al., 2016; Zong et al., 2016). We examined mecciND1 levels in pairs of tumor samples and adjacent tissues from 21 hepatocellular carcinoma (HCC) patients, and mecciND1 was found to be significantly upregulated in HCC (Figure 6F). MecciND5 was also upregulated in HCC, although not as strikingly as mecciND1 (Figure S12C in Supporting Information). MecciRNAs corresponding to *S. pombe* mitochondrial genes (*cox1*, *cob1*, *21S rRNA*) and *C. elegans* mitochondrial genes (*nduo-1*, *nduo-5*, and *ctc-1*) were also identified (Figure S12D and E in Supporting Information). Feeding RNAi targeting *C. elegans* mecci-nduo-5 and mecci-ctc-1 caused defective mitochondrial morphology in body muscles (Figure S12F in Supporting Information), suggesting that mecciRNAs might play critical physiological functions in nematodes.

DISCUSSION

The mutual relations between mitochondria and the "host" cell are a fundamental question in biology. Based on the results from this study and previous findings, a proposed model in which mecciRNAs facilitate the mitochondrial entry of nuclear-encoded proteins through the TOM40 complex is suggested (Figure 7). mecciRNAs may promote the formation of structures favorable to mitochondrial importation by interacting with nascent polypeptides in the cytosol (Figure 5B and C), which is a mechanism of molecular chaperones, as previously known for heat shock proteins (Schmidt et al., 2010). In fact, it has been shown that 5S rRNA acts as a molecular chaperone in the co-importation of 5S rRNA and rhodanese, in which 5S rRNA interacts co-translationally with rhodanese and leads to an enzymatically inactive conformation of rhodanese in human cells, and after which both 5S rRNA and rhodanese are imported to mitochondria (Smirnov et al., 2010).

mecciND1 and mecciND5 interact with TOM40 to facilitate mitochondrial protein entry (Figure 5F), but whether they travel through the TOM40 complex together with their protein partners as a ribonucleoprotein complex remains unknown. It is highly possible that mecciRNAs facilitate the mitochondrial entry of proteins with RNA binding ability, since the process involves interaction between mecciRNAs and the targeted proteins. hnRNPA proteins that act as mecciND5 partners are well established RNA binding proteins (Geuens et al., 2016). RPA proteins that act as mec-

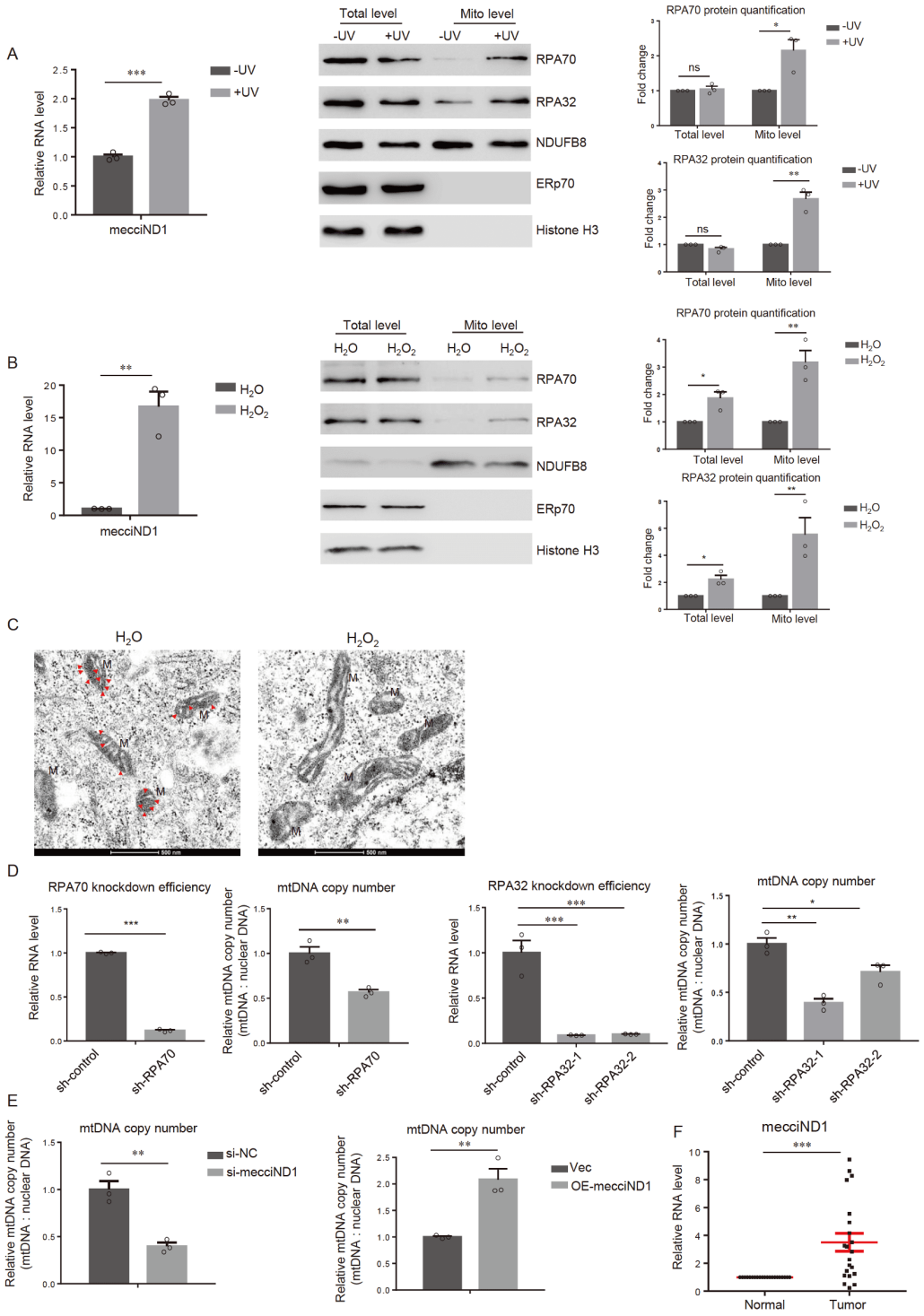

Figure 6 Dynamic expression of mecciND1 and its association with cellular physiology. A, MecciND1 levels and mitochondrial RPA70 and RPA32 protein levels were increased upon UV irradiation in RPE-1 cells. The results of the quantification of RPA proteins are shown (NDUFB8 served as a loading control for mitochondrial proteins; ERp70, an endoplasmic reticulum marker, served as a loading control for whole-cell proteins, and with no UV group as 1.0). B, mecciND1 levels and mitochondrial RPA70 and RPA32 protein levels were increased after H_2O_2 treatment in RPE-1 cells. The results of the quantification of RPA proteins are shown (NDUFB8 served as a loading control for mitochondrial proteins; ERp70, an endoplasmic reticulum marker, served as a loading control for whole-cell proteins, and with H_2O group as 1.0). C, Representative electron microscopy images of immunogold-labelled RPA32 in human RPE-1 cells treated with H_2O_2 (H_2O served as a control). In the H_2O control, RPA32-immunogold particles in the mitochondrion are labelled with red arrowheads. M, mitochondrion. D, Knockdown of RPA70 or RPA32 decreased mitochondrial DNA (mtDNA) copy numbers. The knockdown efficiency of RPA70 and RPA32 at the mRNA level is also shown; sh-control, shRNA with scrambled sequence. E, Copy numbers of mtDNA under mecciND1 knockdown or overexpression. F,mecciND1 levels in pairs of tumour samples and adjacent tissues from 21 hepatocellular carcinoma (HCC) patients. In A, B, D, and F, relative RNA levels determined via qRT-PCR were normalized to 18S rRNA; in A, B, D, and E, n=3 independent experiments; in A, B, and D–F, error bars represent standard error of the mean; ns, not significant; *P<0.05; **P<0.01; ***P<0.001 by Student's t-test.

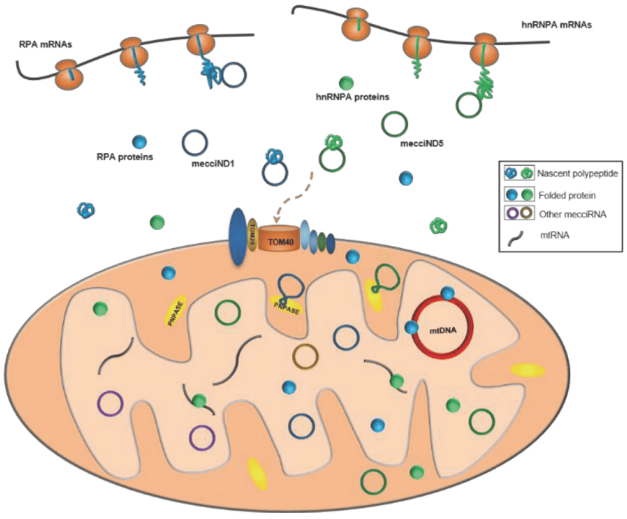

Figure 7 A working model of mecciRNAs in facilitating mitochondrial protein importation. MecciRNAs (e.g., mecciND1 and mecciND5) interact with nascent polypeptides in the cytosol, and then serve as molecular chaperones to promote mitochondrial importation of proteins through the TOM40 complex (e.g., RPA and hnRNPA proteins). PNPASE interacts with the small stem-loop of mecciND1 and mecciND5, and regulates the distribution of mecciRNAs in the mitochondria and cytosol.

ciND1 partners are ssDNA binding proteins with very high affinity (Kd ~10^{-10} mol L^{-1}), although they can also bind to RNA with much lower affinity of ~10^{-6} mol L^{-1} (Kd), which is still reasonable affinity for RNA binding proteins (Brill and Stillman, 1989; Kim et al., 1992). Many so-called non-canonical RNA binding proteins bind RNAs transiently or with low affinity may also be protein partners of specific mecciRNAs (Moore et al., 2018). mtSSB is generally regarded as the mitochondrial ssDNA binding protein, although almost no research has been performed to examine whether RPA proteins also play roles in mitochondria. Previous proteomic investigations have demonstrated the presence of RPA proteins in mitochondria (Smith and Robinson, 2015), and our data directly show the existence and function of RPA proteins in mammalian mitochondria (Figures 2, 3, and 6). Mitochondria require a substantial number of nucleic acid binding proteins encoded by the nuclear genome for their RNA metabolism, transcription, translation, and DNA duplication (Antonicka and Shoubridge, 2015; Calvo et al., 2015; Lopez Sanchez et al., 2011; Zhang et al., 2014). Presumably, most of these proteins bind to multiple types of RNAs in the cytosol, since RNA binding proteins generally exhibit a broader spectrum of RNA targets or are less specific. Allowing mecciRNA-bounded proteins to enter the mitochondria may even serve as a sorting mechanism to ensure the entry of the appropriate types and amounts of proteins and to keep unwanted cytosolic proteins and RNAs from entering the mitochondria. Interestingly, in a recent study, many proteins were found to show aberrant mitochondrial targeting in the absence of SRP, which facilitates protein targeting to the endoplasmic reticulum (Aviram and Schuldiner, 2017; Costa et al., 2018; Walter and Blobel, 1982). There are also g-circRNAs encoded by the nuclear genome in the mitochondria (Figure 1B), and it is possible for them to play similar roles to mecciRNAs in mitochondrial protein importation. The fact that both mecciND1 and mecciND5 overexpressed with plasmids can facilitate the mitochondrial importation of their corresponding target proteins supports this speculation (Figures 3B and 4B; Figures S7C and S8C in Supporting Information).

Another issue is whether each mecciRNA and its protein partner have high specificity to each other. It seems that the RPA proteins and mecciND1 have higher specificity to interact with each other than hnRNPA proteins and mecciND5 (Figures S5C and S6A, Table S2 in Supporting Information). It is also possible that hnRNPA proteins bind to and regulate the metabolism of many mecciRNAs once getting imported primarily by mecciND5 into the mitochondria. The specificity, at least to a certain degree, between mecciRNAs and proteins is further supported by the fact that mecciND5 but not mecciND1 promotes the co-translational importation of hnRNPA1, and mecciND1 compared to mecciND5 has significantly higher promoting effect in the importation of RPA32 protein (Figure S9F and G). What would determine specificity between mecciRNA and the protein cargo remains unclear. It is also possible for mecciRNAs to play roles besides facilitating mitochondrial protein importation. Future studies are needed to further examine the functions of mecciRNAs in mitochondrial protein importation and other potential roles.

MecciRNAs are distributed both inside and outside the mitochondria (Figures 1E, 2E, 2I, 3C, and 4C). We provide *in vitro* indications that mecciRNAs may shuttle in and out of mitochondria (Figure 5A; Figure S9H in Supporting Information), but how they are exported and imported remains elusive. MecciRNAs interact with PNPASE, an enzyme that has been demonstrated to be essential for the mitochondrial importation of RMRP and several other noncoding RNAs (Cheng et al., 2018; Wang et al., 2010). Recently, it was shown that dsRNAs derived from mitochondria play PNPASE-related roles (Dhir et al., 2018). The interaction between PNPASE and mecciRNAs is involved in the protein import role of mecciRNAs (Figure 5F–I). PNPASE may be simply required for the mitochondrial importation and exportation of mecciRNAs, and thus indirectly affect protein importation. PNPASE plays essential roles in mitochondria, and a recent study showed that knockout of the PNPASE gene in cultured cells leads to depletion of mtDNA, after which the cells are eventually depleted of mitochondria (rho0 cells) (Shimada et al., 2018). Elucidation of the relevance of PNPASE to mecciRNAs and mitochondrial protein importation extends the understanding of critical roles of PNPASE.

The junction sites of mecciRNAs resemble those of g-circRNAs generated through backsplicing, although this feature only is not sufficient to suggest a mechanism of backsplicing in the biogenesis of mecciRNAs (Figure 1C; Figure S1B in Supporting Information). There are recent indications of the possible existence of some splicing factors in mammalian mitochondria (Herai et al., 2017). Introns and linear splicing events occur in yeast mitochondria but are generally absent in the mitochondria of multicellular animals (Asin-Cayuela and Gustafsson, 2007; Gaspari et al., 2004; Gray et al., 1999, 2001), and linear splicing was absent in mitochondrial transcripts according to our RNA-seq data. Nuclear-transfected plasmids harboring the corresponding mitochondrial DNA fragment (with the flanking sequences) can successfully overexpress mecciRNAs (Figures 3B and 4B; Figures S7C and S8C in Supporting Information). It is possible that multicellular animals still exhibit mitochondrial splicing in the form of backsplicing to generate mecciRNAs, although mitochondria may lack essential components of linear splicing; the missing components can be due to the lack of real introns on mitochondrial pre-RNA transcripts or may simply be due to the absence of protein factors required in mitochondria. There are also examples in which circRNAs generated from single-exon genes by backsplicing are identified in the nuclear genome, and no linear splicing is involved in the biogenesis of mRNA from single-exon genes (Glažar et al., 2014); for example, the well-known circSry circRNA of mice is encoded by a single-exon gene Sry (Capel et al., 1993; Hansen et al., 2013; Memczak et al., 2013). It is also possible that mecciRNAs are generated via a splicing-independent mechanism. In this context, a related observation is that the majority of circularization events in archaea may be independent of the splicing process (Danan et al., 2011; Patop et al., 2019). The majority of mecciRNAs and the canonical linear mitochondrial transcripts including mRNAs, tRNAs, and rRNAs, are encoded by the heavy strand, which means that mecciRNAs presumably compete with mitochondrial mRNAs, tRNAs, and rRNAs in the biogenesis from the same precursor transcripts. We have also noticed that sites in the RNR1 and RNR2 region are relatively more frequently involved in forming mecciRNA junctions, and the regulatory D loop barely has any mecciRNA forming sites (Figure 1A). The biogenesis and metabolism of mecciRNAs require further elucidation.

Mitochondria need to maintain homeostasis and react to different physiological conditions. Previous studies have focused on how cells "manage" mitochondrial protein importation in response to stresses (Harbauer et al., 2014; Quirós et al., 2015; Sokol et al., 2014; Weidberg and Amon, 2018). It has recently been shown that the mitoCPR (mitochondrial compromised protein import response) mitochondrial initiated surveillance pathway mediates the degradation of unimported proteins from the mitochondrial surface in budding yeast (Weidberg and Amon, 2018). The identification of mitochondrial-encoded mecciRNAs and their physiological roles associated with stress responses and cancer expand our understanding of the complexity of mitochondrial RNAomics as well as the categories and functions of circRNAs (Chen, 2016; Chen et al., 2015; Danan et al., 2011; Hansen et al., 2013; Kristensen et al., 2019; Li et al., 2015; Memczak et al., 2013; Mercer et al., 2011; Patop et al., 2019; Salzman et al., 2012; Szabo and Salzman, 2016; Zhang et al., 2014); mecciRNAs represent another layer of the regulation of mitochondrial physiology and mitochondrion-to-nucleus relations.

MATERIALS AND METHODS

Cell cultures and model organisms

HeLa, HEK293T, RPE-1, HepG2, N2a, and NIH3T3 cells all originated from the ATCC and were cultured with DMEM. All cells were cultured under standard conditions including 10% FBS and 1% penicillin/streptomycin at 37°C under 5% CO_2. Cells were tested for mycoplasma by DAPI staining, to ensure the absence of contamination. *S. pombe* (PR109), N2 wild-type *C. elegans* strain, *D. rerio* (AB, adult male) and 6-week-old male C57BL/6 wild-type mice were cultured according to standard methods. Protocols involving mice and *D. rerio* were approved by the Institutional Animal Care and Use Committee at the University of Science and Technology of China.

Clinical samples

All fresh HCC patient tumor samples and adjacent tissues were collected from The First Affiliated Hospital of University of Science and Technology of China, which was approved by the Human Research Ethics Committee of University of Science and Technology of China (UST-CEC201700007). Written informed consent was obtained from each patient for this study. All samples were rinsed with DEPC water and then kept in RNAhold (Transgene) within 30 min after removing from the operation. HCC patient tumor sample and adjacent tissue pairs were collected from 21 patients (12 males and 9 females with advanced stage HCC, all of them were HBsAg positive, and did not have anti-tumor therapy before surgery) (Sheng et al., 2019).

DNA & RNA isolation, RNase R treatment, and PCR reactions

Genomic and mitochondrial DNA were extracted by RNase A and proteinase K digestion, phenol and chloroform extraction with isopropanol precipitation. Total RNA was extracted with TRIzol Reagent (Invitrogen, USA) according to

the manufacturer's procedures. For RNase R treatment, 5 μg total RNA was treated with 8 U RNase R (Epicentre, USA) in 50 μL total volume for 40 min. Complementary DNA (cDNA) was synthesized from RNA with the GoScript Reverse Transcription System (Promega, USA) according to the supplied protocol, with random hexamer primers. Quantitative PCR (qPCR) was performed with GoTaq SYBR Green qPCR Master Mix (Promega) on a PikoReal 96 real-time PCR system (Thermo Scientific, USA) according to standard procedures. For semi-quantitative PCR, 18–20 amplification cycles were performed.

RNA sequencing

For high-throughput sequencing, RNAs isolated from mitochondria were iron-fragmented at 95°C and then subjected to end repair and 5′-adaptor ligations. Then, reverse transcription was performed with random primers containing 3′-adaptor sequences and randomized hexamers. After cDNA purification and amplification, the PCR products of 200–500 bp were purified and quantified. Libraries were prepared according to the manufacturer's instructions and subjected to 151 nt paired-end sequencing with an Illumina Nextseq 500 system. We sequenced each library to a depth of 10–50 million read pairs and then removed adapters with cutadapt to obtain clean reads.

DNA re-sequencing

The extracted genomic or mitochondrial DNA was sequenced using the HiSeq 2500 sequencing systems (Illumina Inc., https://www.illumina.com). In short, the obtained reads were mapped to hg19 reference genome with bowtie (-v 1) and PCR amplifications were performed with PICARD.

MecciRNA identification and g-circRNA identification

For mecciRNA annotation, the pipeline of find_circ (Memczak et al., 2013) was applied with reference genome (human: hg19; mouse: mm9; zebra: danRer11) downloaded from the UCSC genome browser (http://genome.ucsc.edu/). In brief, we aligned reads to the reference genome and filtered reads that aligned contiguously; for the remaining reads, we extracted 20-mers from both ends and aligned them independently to find unique anchor positions in chrM (mitochondrial genome), and then we extended the anchor alignments of two read segments mapping to chrM in the reversed order. Only circRNAs with ≥2 junction reads across four human samples or four mouse samples were analyzed. For zebrafish with only one sample sequenced, circRNAs with ≥1 junction reads were analyzed. g-circRNAs (circRNAs encoded by the nuclear genome) were identified with find_circ.

Motif identification

The enriched motifs of junctions (-len 10) and flanking site sequences (-len 20) for mecciRNAs were generated by HOMER.

Linear splicing identification in mitochondrial transcripts

For linear splicing, we first aligned the RNA-seq data to the reference genome with bowtie (-v 1) to filter the contiguously mapped reads. Then, we mapped the remaining reads to chrM with blat to find the *de novo* split transcripts in mitochondria.

Northern blotting

Sense and antisense digoxigenin-labeled RNA probes were prepared with a DIG Northern Starter Kit (Roche, Germany) according to the manufacturer's protocol. 20 μg of total RNA with or without RNase R digestion and RiboRuler Low Range RNA Ladder (Thermo Scientific) were loaded in 8% Urea PAGE gel and run for 1 h in 1× TBE buffer. RNA was transferred onto Hybond-N+ membranes (GE Healthcare, USA) by electronic transfer. After transfer, the membranes were UV-crosslinked and hybridized with specific RNA probes according to the manufacturer's protocol (Roche, DIG Northern Starter Kit). Images were taken with an ImageQuant LAS4000 Biomolecular Imager (GE Healthcare) (Wang and Shan, 2018).

Plasmid construction

All plasmids were constructed with restriction-enzyme digestion (Thermo Scientific FD) and ligation (Promega A3600) or with recombinant methods (Vazyme, China, c112-02). Oligonucleotide sequences for primers used in plasmid construction, probe preparation, siRNAs, and biotin-labeled nucleic acids are listed in Table S3 in Supporting Information. The shRNA plasmid for knockdown of hRPA70 mRNA (shRPA70, TRCN0000010985), hRPA32 mRNA (shRPA32-1, TRCN0000005986; shRPA32-2, TRCN0000005987) with negative-control shRNA (shC002) was obtained from the MISSION shRNA Library (Sigma-Aldrich, Germany). For the overexpression of C-terminal FLAG-tagged TOM20, TOM40 and PNPASE the plasmid backbone was pmR-mCherry. The structures of overexpression plasmids of human mecciND1 and mecciND5 are shown in Figures S7C and S8C in Supporting Information. The major constructions of plasmids used for *in vitro* assays (Wesselhoeft et al., 2018) are shown in Figure S9B in Supporting Information. Purified mecciND1, mecciND5, circSRSF, and RMRP fragments from PCR reactions and chemically synthesized group I self-

splicing intron were cloned into pUC57 vector. Coding sequence of RPA32 or hnRNPA1 fused with sequence corresponding to FLAG tag at the 3′ terminal was inserted downstream of the SP6 promoter in pcDNA3 plasmid. *C. elegans* plasmid, myo-3p::tomm20(aa1-49)::GFP, was constructed for visible mitochondrial network of muscle cells (Weir et al., 2017). Feeding RNAi plasmids were constructed by inserting the amplified fragments (100–200 bp junction sequences of the corresponding mecciRNAs) into L4440 vector (Addgene, USA). All plasmids were sequenced for confirmation.

RNA pull-down with biotin-labeled antisense oligonucleotides

RNA pull-down with 5′-biotinylated antisense (AS) oligos was modified with a previously described method (Hu et al., 2016). Briefly, cells were cross-linked for 2 min in a UV cross-linker (UVP) at 120 mJ cm^{-2} strength. The cross-linked cells or purified mitochondria were then lysed in RIPA buffer (50 mmol L^{-1} Tris-HCl, pH 8.0, 150 mmol L^{-1} NaCl, 5 mmol L^{-1} EDTA, 1% NP-40, 0.1% SDS), 2 mmol L^{-1} DTT, 1X protease-inhibitor cocktail (Roche) and 200 units mL^{-1} RNasin® Ribonuclease Inhibitors (Promega) for 10 min on ice, then sonicated for 10 min with a Sonics Vibra-Cell. Lysates were cleared of cell debris by centrifugation at 13,000×*g* for 15 min. 100 pmol biotinylated AS oligos was added to the supernatant and mixed by end-to-end rotation at room temperature for 2 h. M-280 Streptavidin Dynabeads (Life Technologies, USA) were blocked with 500 ng μL^{-1} yeast tRNA and 500 ng μL^{-1} BSA for 1 h at room temperature, then washed with RIPA buffer before being resuspended. 50 μL blocked Dynabeads was added per 100 pmol of biotin-DNA oligonucleotides, and the mixture was then rotated for 2 h at room temperature. Beads were captured with magnets (Life Technologies) and washed two times with RIPA buffer and two times with RIPA buffer supplemented with 500 mmol L^{-1} NaCl, for mecciND1 pull down (and the corresponding scramble control) we washed 3 times with RIPA buffer and 3 times with RIPA buffer supplemented with 500 mmol L^{-1} NaCl. RNAs and proteins were eluted from beads for further analysis. Proteins pulled down by AS oligos were separated on SDS-PAGE gels, and silver-stained.

Mass spectrometry

Specific silver-stained bands were cut, digested and extracted. The masses of the peptides in the extract were then measured by MS to obtain the peptide mass fingerprints. Next, peptides were selected to undergo fragmentation via tandem MS. Both the MS and tandem MS data were searched against protein sequence databases to determine the proteins present in the gel.

RNA Immunoprecipitation (RIP)

RIP was carried out as previously described with some modifications (Li et al., 2015). Briefly, cells were cross-linked in a UV cross-linker (UVP) at 120 mJ cm^{-2} strength, and then harvested in ice-cold RIPA buffer (50 mmol L^{-1} Tris-HCl, pH 8.0, 150 mmol L^{-1} NaCl, 5 mmol L^{-1} EDTA, 1% NP-40, 0.1% SDS), 200 units mL^{-1} RNasin® Ribonuclease Inhibitors (Promega), 2 mmol L^{-1} DTT, and 1X protease-inhibitor cocktail (Roche). Cells were sonicated for 10 min with a Sonics Vibra-Cell, the cell suspension was centrifuged at 13,000×*g* for 15 min at 4°C, and the supernatant was collected. Antibody or IgG (as control) was added and incubated 4 h at 4°C for antigen coupling, and then Protein G Dynabeads (Life Technology) suspension was then added and allowed to bind for at least 2 h at 4°C. The protein-antibody–beads complexes were washed two times with RIPA buffer and two times with RIPA buffer supplemented with 500 mmol L^{-1} NaCl. One-fifth of the beads after the last wash was heated 100°C for 10 min in SDS-loading buffer and then saved for Western blotting. The remaining protein-antibody–beads complexes were digested with proteinase K at 55°C for 30 min, followed by extraction with TRIzol Reagent to obtain RNA. The following antibodies were used: anti-RPA70 (Abcam, UK, ab79398); anti-RPA32 (Abcam, ab2175); anti-hnRNPA1 (Sigma-Aldrich, R4528); anti-FLAG (Sigma-Aldrich, F1804). Antibody validation is provided on the manufacturers' website.

Western blotting

For Western blotting, whole cell lysates, mitochondria lysates, and IP mixtures were separated on SDS-PAGE gels and then transferred to BioTrace NT Nitrocellulose Transfer Membrane (PALL Co., USA). Membranes were processed according to the ECL Western Blotting protocol (GE Healthcare). The following antibodies were used in Western blotting: anti-RPA70 (Abcam, ab79398); anti-RPA32 (Abcam, ab2175); anti-hnRNPA1 (Sigma-Aldrich, R4528); anti-hnRNPA2B1 (Abcam, ab6102), anti-hnRNPA3 (Proteintech Group, USA, 25142-1-AP); anti-GAPDH (Proteintech Group, 60004-1-IG); anti-ERp70 (Proteintech Group, 14712-1-AP); anti-NDUFB8 (Proteintech Group, 14794-1-AP); anti-TOM20 (Proteintech Group, 11802-1-AP), anti-TOM40 (Proteintech Group, 18409-1-AP); anti-TIM23 (Proteintech Group, 11123-1-AP); anti-FLAG (Sigma-Aldrich, F1804); anti-β-actin (Transgene, China, HC201); Anti-PNPT1 (Abacm, ab96176). Antibody validation is provided on the manufacturer's website. Quantification of Western blot bands was performed with Image J.

Immunofluorescence (IF) combined with fluorescence *in situ* hybridization (FISH)

FISH probes were generated with Transcript Aid T7 High

Yield Transcription Kit (Thermo Scientific), and then labeled with Alexa Fluor546, 488 or 647, by using the ULYSIS Nucleic Acid Labeling Kit (Invitrogen), which added a fluor on every G in the probe to amplify the fluorescence intensity. HeLa cells or RPE-1 cells were grown on coverslips, fixed in 3% PFA for 10 min at room temperature, and then permeabilized with freshly made PBS, 1% v/v Triton X-100 (plus 200 units μL^{-1} RNase inhibitor) on ice for 10 min. Then they were blocked in 1% w/v BSA for 30 min at room temperature, incubated with primary antibody 1:100 diluted in 1% BSA (containing 200 units mL^{-1} RNase inhibitor) for 3 h at room temperature, washed with PBS, 0.1% Triton X-100 for three times, incubated with secondary antibody (1:200 diluted in 1% BSA, containing 200 units mL^{-1} RNase inhibitor) for 1 h at room temperature in a dark and humid chamber (made with paper tissues soaked with PBS), washed with PBS, 0.1% Triton X-100 for three times (dark), and washed with 2× SSC (Sigma-Aldrich) once (dark). RNA probes were denatured at 80°C for 10 min with 30 ng μL^{-1} Salmon DNA (Invitrogen) and 500 ng μL^{-1} yeast tRNA (Invitrogen) in 2× hybridization buffer (4× SSC, 40% w/v dextran sulfate). After denature, 200 units mL^{-1} RNase inhibitor was added in the mixture and slides were put on. The mixture was hybridized overnight at 37°C in a dark and humid chamber (made using paper tissues soaked in 50% v/v formamide in 2× SSC). Slides were washed with 2× SSC 0.1% Triton X-100 at 45°C; the DNA was counterstained with DAPI. Cover-slide was then mounted. The following antibodies were used in IF: anti-RPA70 (Abcam, ab79398); anti-RPA32 (Abcam, ab2175); anti-hnRNPA1 (Sigma-Aldrich, R4528); anti-hnRNPA2B1 (Abcam, ab6102), anti-hnRNPA3 (Proteintech Group, 25142-1-AP); anti-TOM20 (Proteintech Group, 11802-1-AP; Abcam, ab56783), anti-TOM40 (Proteintech Group, 18409-1-AP). Donkey anti-Mouse Secondary Antibody, Alexa Fluor 488 (Invitrogen, A21202), Donkey anti-Rabbit IgG Secondary Antibody, Alexa Fluor 546 (Invitrogen, A10040), Goat Anti-Rabbit Secondary Antibody Alexa Fluor® 488 (Abcam, ab181448), Goat Anti-Mouse Secondary Antibody Chromeo™ 546 (Abcam, ab60316). Antibody validation is provided on the manufacturers' websites.

Transfection of plasmids, siRNAs, and AMOs

Plasmid and siRNA transfection were conducted with Lipofectamine 2000 (Invitrogen) according to the supplier's protocols. All siRNAs were subjected to BLAST search to ensure the absence of hits with more than 17 nt matches in the corresponding genomes. For co-transfection of PNPASE-FLAG plasmid and wt/mut mecciND1 or mecciND5 overexpression plasmid, PNPASE-FLAG plasmid was transfected first for 12 h and wt/mut mecciND1 or mecciND5 overexpression plasmid was transfected for another 48 h. Antisense Morpholino oligonucleotides (AMOs), including mecciND1 AMO, mecciND5 AMO, and scrambled AMO, were synthesized at Gene Tools, USA, and the AMO targets predicted single-stranded region of mecciND1 or mecciND5. AMOs were transfected through electroporation with the NucleofectorTM system (Lonza, Switzerland) according to the manufacturer's instructions. Cells were harvested for analysis or downstream experiments 8–12 h after AMO transfection. The final concentration of AMOs was 10 $\mu mol\ L^{-1}$.

Quantification of mecciRNA copy number per cell

DNA fragments corresponding to human mecciND1 and mecciND5 were amplified through RT-PCR reactions with divergent primers (to amplify mecciRNA only). The purified DNA fragments were diluted by grads multiple to plot standard curves through real-time PCR. Total RNAs from 1.0×10^6 HeLa, 293T, RPE-1 and HepG2 cells were extracted, and cDNAs were then synthesized. The mecciND1 and mecciND5 copy numbers per cell in each cell line were calculated on the basis of cell numbers and the C_t values from the qRT-PCR using the standard curves.

UV, H_2O_2, TM, and hypoxia treatment of cells

For UV irradiation, cells were first grown to reach 80%–90% confluency. Then the culture medium was discarded, and cells were either left untreated (negative control) or exposed to 25 $mJ\ cm^{-2}$ UVC irradiation. Cells were then washed with PBS and placed in fresh media, and then incubated for 30–60 min before harvest. For H_2O_2 treatment, cells were first grown to reach 80%–90% confluency in complete medium and the culture medium was subsequently replaced with DMEM without FBS, together with or without 1 $mmol\ L^{-1}$ H_2O_2. Cells were then incubated for 1 h before harvest. For TM (tunicamycin) treatment, cells were treated with 100 $mg\ mL^{-1}$ TM for 4 h. Cells exposed to hypoxia were maintained at 1% O_2/5% CO_2/balance N_2 at 37°C in a modular incubator chamber for 24 h.

Mitochondria isolation

Mitochondria isolation of the cultured cells was carried out as previously described with some modifications (Wieckowski et al., 2009; Williamson et al., 2015). Briefly, cells were harvested and washed by PBS, collected by centrifugation and re-suspended in ice-cold isolation buffer 1 (225 $mmol\ L^{-1}$ mannitol, 75 $mmol\ L^{-1}$ sucrose, 0.1 $mmol\ L^{-1}$ EGTA and 20 $mmol\ L^{-1}$ HEPES-KOH, pH 7.4). Cells were homogenized by 20 strokes in a Dounce homogenizer (Kontes, USA). Cell homogenates were centrifuged twice at 1,500×*g* at 4°C for 5 min to discard the nucleus and collect clear supernatant. Mitochondria were

sedimented at 12,000×*g* at 4°C for 10 min. The ER contaminant proteins make a large, loose white ring around the more stable mitochondrial pellet. The mitochondrial pellet appeared more yellow in color. This was then gently washed with isolation buffer 2 (225 mmol L^{-1} mannitol, 75 mmol L^{-1} sucrose, and 20 mmol L^{-1} HEPES-KOH, pH 7.4) until the white ring was washed out. Mitochondria isolation of animal tissues was carried out as previously described with some modifications (Wieckowski et al., 2009). Briefly, tissues were washed in ice-cold IB-1 (225 mmol L^{-1} mannitol, 75 mmol L^{-1} sucrose, 0.5% BSA, 0.5 mmol L^{-1} EGTA and 20 mmol L^{-1} HEPES-KOH, pH 7.4), cut into small pieces using scissors in ice-cold IB-3 (225 mmol L^{-1} mannitol, 75 mmol L^{-1} sucrose and 20 mmol L^{-1} HEPES-KOH, pH 7.4) and washed once again with 10 mL fresh ice-cold IB-1. The tissue fragments were resuspended with IB-1 in the ratio 4 mL of buffer per gram of tissue, transferred to the glass tissue homogenizer for homogenization, and then the homogenates were again homogenized in a Dounce homogenizer (Kontes) by 20 strokes. The centrifugation procedures were the same as that described in the procedure for mitochondria isolation of the cultured cells. Zebrafish mitochondria isolation is similar to that for the tissue. Briefly, the zebrafish was put on ice for 1 min, washed in ice-cold IB-1, cut into small pieces using scissors in ice-cold IB-3. The following procedures were the same as described in the procedure for mitochondria isolation of the cultured cells.

Isolation of mitochondrial RNAs & proteins and cytosolic RNAs

The purified mitochondria for RNA-seq were then treated with 100 mg mL^{-1} RNase A for 10 min on ice following 1 mg mL^{-1} Digitonin (Sigma) for another 10 min to remove contaminating cytoplasmic RNA. The purified mitochondria for Western blotting were treated with 1 mg mL^{-1} Digitonin (Sigma) for 10 min to remove contaminating protein. Both Western blotting and RT-qPCR were carried out to confirm the quality of purified mitochondria. For cytosolic RNA isolation, the supernatants after precipitation of mitochondria were centrifuged again at 15,000×*g* at 4°C for 10 min followed by extraction with TRIzol LS reagent to obtain RNA.

In vitro transcription and circularization

Templates of *in vitro* transcription were amplified by specific primers containing T7 RNA polymerase promoter sequences from the vectors described above. Linear RNA or circRNA precursor was synthesized by *in vitro* transcription using a TranscriptAid T7 High Yield Transcription Kit (Thermo Scientific). After *in vitro* transcription, reactions were treated with DNase I for 20 min. After DNase treatment, linear RNA was purified using Phenol-chloroform pH ~4.5. For circRNA, the procedures of *in vitro* circularization are shown in Figure S9B in Supporting Information and circularization was carried out as previously described with some modifications (Wesselhoeft et al., 2018). Briefly, after DNase treatment, additional GTP was added to a final concentration of 2 mmol L^{-1} along with a circularization buffer including magnesium (15 mmol L^{-1} $MgCl_2$, 1 mmol L^{-1} DTT, 50 mmol L^{-1} Tris-HCl, pH 7.5), and then the reaction was heated at 55°C for 20 min. RNA was then purified using phenol-chloroform, pH ~4.5. To enrich for circRNA, 10 μg RNA was digested with RNase R and then phenol-chloroform purified. RNase R digested RNA was separated on 5% Urea PAGE gel. Bands corresponding to circRNA were excised from the gel and eluted overnight in elution buffer (20 mmol L^{-1} Tris-HCl, pH 7.5, 250 mmol L^{-1} NaOAc, 1 mmol L^{-1} EDTA, 0.25% SDS). After elution, the gel fragments were discarded by centrifugation at 15,000×*g* at 4°C for 2 min. RNA was then purified using phenol-chloroform, pH ~4.5. As shown in Figure S9B in Supporting Information, the circRNAs (including the circRNA control) *in vitro* synthesized could be examined from the endogenous circRNAs due to a small stretch of added sequences (29 nt).

Importation of RNAs into isolated mitochondria

Mitochondria were isolated from 293T cells. The isolated mitochondria were resuspended in import buffer (250 mmol L^{-1} Sucrose, 20 mmol L^{-1} HEPES-KOH, pH 7.4, 5 mmol L^{-1} $MgCl_2$, 60 mmol L^{-1} KCl, 2 mmol L^{-1} ATP, 10 mmol L^{-1} Succinate, 1 mmol L^{-1} DTT). After incubation for 15 min at 30°C, the mitochondria (~25–50 μg of total mitochondrial proteins) were divided equally into the import system. 200 ng linear RNA or circular RNA with import buffer was added into the system to the final volume of 100 μL. The import reaction was performed at 30°C for 30 min with shaking gently several times. After the reaction, 3,500 gel units Micrococcal Nuclease (NEB, USA) together with its reaction buffer were added to eliminate RNAs that were not imported into mitochondria, and then the mixture was incubated at 30°C for 20 min. Mitochondria were then spun down at 13,000×*g* at 4°C for 5 min. After 2 times wash with isolation buffer 2, the mitochondrial pellets were dissolved in TRIzol Reagent for RNA.

In vitro mitochondrial importation of proteins

Capped RPA32-FLAG and hnRNPA1-FLAG mRNAs were *in vitro* transcribed from linearized SP6 plasmids using the mMESSAGE mMACHINE™ SP6 Transcription Kit (Invitrogen) according to manufacturer's directions. After transcription, *E. coli* poly(A) polymerase (NEB) was added into reaction for poly(A) tailing of capped-mRNA. For *in vitro* importation of RPA32-FLAG protein together with

mecciND1 or hnRNPA1-FLAG protein together with mecciND5 (co-translation), isolated mitochondria were resuspended in the import buffer and incubated for 15 min at 30°C. 200 ng circularized mecciND1, mecciND5, circSRSF (g-circRNA control), or no circRNA control along with 2 μg RPA32-FLAG or hnRNPA1-FLAG mRNA were added into Rabbit Reticulocyte Lysate System (Promega) for 1 h. 5 μL of the mixture was then taken out as input. The mitochondria (~25–50 μg of total mitochondrial proteins) were divided equally into the three translation systems to a final volume of 50 μL at 30°C for 1 h. To reveal possible earlier difference in co-translational transportation, the import was performed for 30 min (Figure S9F and G in Supporting Information). 3,500 gel units Micrococcal Nuclease (NEB) together with its reaction buffer were added into the mixture, and then incubated at 30°C for 20 min to digest all RNAs not in the mitochondria. Mitochondria were then spun down at 13,000×*g* at 4°C for 5 min and resuspended with 100 μL import buffer. The samples were treated with 25 μg mL^{-1} Trypsin for 5 min at room temperature to digest any protein outside of the mitochondria, and then trypsin was stopped by 1 mmol L^{-1} TLCK (Sigma) and Soybean Trypsin Inhibitor (BI, Israel). Mitochondria were spun down again at 13,000×*g* at 4°C for 5 min. After 2 times wash with isolation buffer 2, 1/4 of the mitochondrial pellets was taken out for RNA isolation and the left was subjected to Western blotting. For the "post-translation" effects of mecciRNAs, 2 μg RPA32-FLAG or hnRNPA1-FLAG mRNA was added into Rabbit Reticulocyte Lysate System (Promega) in a total volume of 50 μL for 30 min at 30°C, and then 5 μL of the mixture was taken out as input. The remaining materials were incubated with 200 ng circularized mecciND1, mecciND5, circSRSF (g-circRNA control), or no circRNA control for 15 min at 30°C, following the addition of isolated mitochondria (pre-warmed in the import buffer for 15 min at 30°C). The mitochondria (~25–50 μg of total mitochondrial proteins) were divided equally into the three reactions to a final volume of 100 μL at 30°C for 1 h.

RNA export assay

RNA export assay was carried out as previously described with some modifications (Wang et al., 2010). After the assays of mecciND1, mecciND5 or circSRSF RNA importation into isolated mitochondria, the mitochondria were then subjected to Micrococcal Nuclease treatment of 3,500 gel units Micrococcal Nuclease (NEB) together with its reaction buffer at 30°C for 20 min. 10 mmol L^{-1} EGTA was then added to inactivate the Micrococcal Nuclease, and the mitochondria were spun down at 13,000×*g* at 4°C for 10 min. The supernatant was removed, and the mitochondrial pellet was washed with 1 mL pre-warmed (30°C) isolation buffer 2. The pellet was then resuspended in 160 μL pre-warmed (30°C) simpler import buffer (250 mmol L^{-1} Sucrose, 20 mmol L^{-1} HEPES-KOH, pH 7.4, 2 mmol L^{-1} ATP, 10 mmol L^{-1} Succinate). For 0 min sample (before the export assay), 80 μL mixture was taken out and spun at 13,000×*g* at 4°C for 10 min, and both the supernatant and pellet were kept for RNA isolation. 20 μL Rabbit Reticulocyte Lysate was added into the 80 μL mitochondria in the simpler import buffer, and the export reaction was performed at 30°C for 20 min with gentle shakes several times. After export, the reaction system was spun at 13,000×*g* at 4°C for 10 min. Both the supernatant and pellet were then subjected to RNA isolation.

Mitochondria DNA copy number

The relative mtDNA copy number was calculated as a ratio of mtDNA/nuclear DNA according to a previous study (Venegas and Halberg, 2012). Briefly, cells were lysed in the RIPA buffer and DNA extracted with phenol/chloroform followed by ethanol precipitation. For quantification of mtDNA, a pair of primers (mtDNA forward and mtDNA reverse) that target the tRNA-Leu (UUR) gene were used for qPCR. To quantify nuclear DNA, we used a pair of primers (nucDNA forward and nucDNA reverse) that target the nuclear β2-microglobulin gene for qPCR.

Feeding RNAi

RNAi plasmids and L4440 vector control (Addgene) were used to transform competent HT115 (DE3) bacteria. Feeding RNAi was performed as previously described (Liu et al., 2012; Shan, 2010). Briefly, each RNAi colony was grown overnight for 15–17 h in LB with 100 mg mL^{-1} ampicillin and then seeded onto NGM plates containing 1 mmol L^{-1} isopropylthiogalactoside (IPTG) to induce dsRNA expression overnight at room temperature. Worms expressing GFP targeted to the outer mitochondrial membrane were synchronized via bleaching using gravid adults. Total RNA was digested with RNase R first for detection of mecciRNA knockdown efficiency by feeding RNAi.

Confocal microscopy

IF-FISH images were taken on a Zeiss LSM 880 confocal microscope with 63× 1.40 NA oil-immersion objective. z-stack images were acquired with a resolution of 1,024×1,024 using ZEN Black confocal software (Zeiss, Germany). The images were saved as .czi files and converted to .tiff files using ZEISS ZEN microscope software. Each .tiff file was processed in the open-source image processing software, (Fiji is Just) Image J. The ROI was drawn as a small rectangle and colocalization percentage of proteins and RNAs in 20 ROIs was measured using image J plugin Coloc2. Z

project was processed by Image J. Imaging of *C. elegans* muscle cell mitochondrial network was performed on Olympus IX-71 inverted microscope (Olympus Corporation, Japan) with 60 1.45 NA oil-immersion objective, and the 14-bit digital images were acquired by an Andor iXonEM+ DV897K EM CCD camera. The images were saved as .tiff files. Z project was processed by image J. Images were from day-1 adult anesthetized for 20 min in 0.2 mg mltetramisole (in M9 buffer) and mounted on 2% agarose pads on glass slides under cover-slides.

Structured illumination microscopy (N-SIM)

Structured illumination microscopy (SIM) super-resolution images were taken on a Nikon N-SIM system with a 100× oil immersion objective lens, 1.49 NA (Nikon, Japan). Images were captured using Nikon NIS-Elements and reconstructed using slice reconstruction in NIS-elements. Images of fixed cells for 3D N-SIM were taken using Z -stacks with step sizes of 0.2 μm. The images were saved as .tiff files. Z project was processed by Image J. Fluorescence quantification of mecciND1, RPA32, mecciND5, and hnRNPA1 in RPE-1 cells was processed by Image J. Briefly, we selected a mitochondrion with a square and measured FISH signal (M, magenta) and protein signal (G, green) separately in this square. Thirty (for RPA32 and meeciND1) and 39 (for hnRNPA1 and mecciND5) mitochondrial areas were randomly selected for fluorescence quantification.

Immuno-electron microscopy

HeLa cells were grown in 6 cm dishes and H_2O_2 treated as described above, trypsinized and pelleted for 2 min at 1,000×*g*. Cells were then washed two times in PBS and then fixed in a solution containing 3.0% formaldehyde, 2% glutaraldehyde in 0.1 mol L^{-1} PBS (pH 7.4) and subsequently osmicated in Palade's OsO_4 for 1.5 h. The fixed cells were dehydrated through a graded series of ethanol and embedded in resin. Sections were cut on a Leica Ultracut UCT ultramicrotome. 70 nm sections were transferred to 200-mesh Formvar and carbon-coated copper grids and then immunolabeled as follows. Grids were placed on 1% H_2O_2 at room temperature for 10 min, and washed 3 times (5 min each) in water. After 10 min in 1% Tween-20/phosphate buffer, the grids were placed on 50 mmol L^{-1} glycine in PBS for 15 min at room temperature. The grids were blocked in blocking solution (5% BSA, 5% goat serum, and 0.1% Tween-20 in PBS) for 30 min at room temperature, and then incubated on a droplet of primary (RPA32) antibody diluted 1:25 in incubation buffer (2.5% BSA, 1% goat serum, 0.1% Tween-20 in PBS) for 2 h at room temperature. Grids were washed 5 times (5 min each) in incubation buffer, then incubated with secondary antibody (AURION, 25132, Netherlands, Goat-anti-Mouse IgG (H&L) EM-grade 15 nm) diluted 1:20 in incubation buffer for 90 min at room temperature, and then washed 5 times (5 min each) in incubation buffer. The grids were post-fixed with 2% glutaraldehyde in PBS for 5 min followed by three times of washes (5 min each) with PBS and three washes (5 min each) with filtered water. Grids were then post-stained for 10 min with uranyl acetate and Reynold's lead citrate and analyzed using a Tecnai G2 Spirit BioTWIN transmission electron microscope (FEI, USA). The images were analyzed by Image J software.

Statistical analysis

Either Student's *t*-tests or Mann-Whitney *U* tests were used to calculate *P* values, as indicated in the figure legends. For Student's *t*-tests, the values reported in the graphs represent averages of three independent experiments, with error bars showing standard error of the mean. After analysis of variance with *F* tests, the statistical significance and *P* values were evaluated with Student's *t*-tests. Statistical methods are also indicated in the figure legends.

Data availability

All RNA-seq and DNA resequencing data are deposited in the NCBI with the accession number.

Compliance and ethics *The author(s) declare that they have no conflict of interest.*

Acknowledgements *We thank Lei Liu for technical support of C. elegans experiments. This work was supported by grants to G. S.: the National Key R&D Program of China (2019YFA0802600 and 2018YFC1004500), the National Natural Science Foundation of China (31725016, 31930019, and 91940303), and the Strategic Priority Research Program (Pilot Study) "Biological basis of aging and therapeutic strategies" of the Chinese Academy of Sciences (XDPB10).*

References

Anderson, S., Bankier, A.T., Barrell, B.G., de Bruijn, M.H.L., Coulson, A. R., Drouin, J., Eperon, I.C., Nierlich, D.P., Roe, B.A., Sanger, F., et al. (1981). Sequence and organization of the human mitochondrial genome. Nature 290, 457–465.

Antonicka, H., and Shoubridge, E.A. (2015). Mitochondrial RNA granules are centers for posttranscriptional RNA processing and ribosome biogenesis. Cell Rep 10, 920–932.

Asin-Cayuela, J., and Gustafsson, C.M. (2007). Mitochondrial transcription and its regulation in mammalian cells. Trends Biochem Sci 32, 111–117.

Aviram, N., and Schuldiner, M. (2017). Targeting and translocation of proteins to the endoplasmic reticulum at a glance. J Cell Sci 130, 4079–4085.

Bao, X., Guo, X., Yin, M., Tariq, M., Lai, Y., Kanwal, S., Zhou, J., Li, N., Lv, Y., Pulido-Quetglas, C., et al. (2018). Capturing the interactome of newly transcribed RNA. Nat Methods 15, 213–220.

Boos, F., Krämer, L., Groh, C., Jung, F., Haberkant, P., Stein, F.,

Wollweber, F., Gackstatter, A., Zöller, E., van der Laan, M., et al. (2019). Mitochondrial protein-induced stress triggers a global adaptive transcriptional programme. Nat Cell Biol 21, 442–451.
Brill, S.J., and Stillman, B. (1989). Yeast replication factor-A functions in the unwinding of the SV40 origin of DNA replication. Nature 342, 92–95.
Calvo, S.E., Clauser, K.R., and Mootha, V.K. (2015). MitoCarta2.0: an updated inventory of mammalian mitochondrial proteins. Nucleic Acids Res 44, D1251–D1257.
Capel, B., Swain, A., Nicolis, S., Hacker, A., Walter, M., Koopman, P., Goodfellow, P., and Lovell-Badge, R. (1993). Circular transcripts of the testis-determining gene Sry in adult mouse testis. Cell 73, 1019–1030.
Chen, L.L. (2016). The biogenesis and emerging roles of circular RNAs. Nat Rev Mol Cell Biol 17, 205–211.
Chen, L., Huang, C., Wang, X., and Shan, G. (2015). Circular RNAs in eukaryotic cells. CG 16, 312–318.
Cheng, Y., Liu, P., Zheng, Q., Gao, G., Yuan, J., Wang, P., Huang, J., Xie, L., Lu, X., Tong, T., et al. (2018). Mitochondrial trafficking and processing of telomerase RNA TERC. Cell Rep 24, 2589–2595.
Costa, E.A., Subramanian, K., Nunnari, J., and Weissman, J.S. (2018). Defining the physiological role of SRP in protein-targeting efficiency and specificity. Science 359, 689–692.
Danan, M., Schwartz, S., Edelheit, S., and Sorek, R. (2011). Transcriptome-wide discovery of circular RNAs in Archaea. Nucleic Acids Res 40, 3131–3142.
Deshaies, R.J., Koch, B.D., Werner-Washburne, M., Craig, E.A., and Schekman, R. (1988). A subfamily of stress proteins facilitates translocation of secretory and mitochondrial precursor polypeptides. Nature 332, 800–805.
Dhir, A., Dhir, S., Borowski, L.S., Jimenez, L., Teitell, M., Rötig, A., Crow, Y.J., Rice, G.I., Duffy, D., Tamby, C., et al. (2018). Mitochondrial double-stranded RNA triggers antiviral signalling in humans. Nature 560, 238–242.
Gaspari, M., Larsson, N.G., and Gustafsson, C.M. (2004). The transcription machinery in mammalian mitochondria. Biochim Biophys Acta Bioenerg 1659, 148–152.
Geuens, T., Bouhy, D., and Timmerman, V. (2016). The hnRNP family: insights into their role in health and disease. Hum Genet 135, 851–867.
Glažar, P., Papavasileiou, P., and Rajewsky, N. (2014). circBase: a database for circular RNAs. RNA 20, 1666–1670.
Gray, M.W., Burger, G., and Lang, B.F. (1999). Mitochondrial evolution. Science 283, 1476–1481.
Gray, M.W., Burger, G., and Lang, B.F. (2001). The origin and early evolution of mitochondria.. Genome Biol 2, reviews1018.1.
Gustafsson, C.M., Falkenberg, M., and Larsson, N.G. (2016). Maintenance and expression of mammalian mitochondrial DNA. Annu Rev Biochem 85, 133–160.
Hansen, T.B., Jensen, T.I., Clausen, B.H., Bramsen, J.B., Finsen, B., Damgaard, C.K., and Kjems, J. (2013). Natural RNA circles function as efficient microRNA sponges. Nature 495, 384–388.
Harbauer, A.B., Zahedi, R.P., Sickmann, A., Pfanner, N., and Meisinger, C. (2014). The protein import machinery of mitochondria—a regulatory hub in metabolism, stress, and disease. Cell Metab 19, 357–372.
Herai, R.H., Negraes, P.D., and Muotri, A.R. (2017). Evidence of nuclei-encoded spliceosome mediating splicing of mitochondrial RNA. Hum Mol Genet 26, 2472–2479.
Herst, P.M., Rowe, M.R., Carson, G.M., and Berridge, M.V. (2017). Functional mitochondria in health and disease. Front Endocrinol 8, 296.
Hu, S., Wang, X., and Shan, G. (2016). Insertion of an Alu element in a lncRNA leads to primate-specific modulation of alternative splicing. Nat Struct Mol Biol 23, 1011–1019.
Kim, C., Snyder, R.O., and Wold, M.S. (1992). Binding properties of replication protein A from human and yeast cells.. Mol Cell Biol 12, 3050–3059.
Kristensen, L.S., Andersen, M.S., Stagsted, L.V.W., Ebbesen, K.K., Hansen, T.B., and Kjems, J. (2019). The biogenesis, biology and characterization of circular RNAs. Nat Rev Genet 20, 675–691.
Li, Z., Huang, C., Bao, C., Chen, L., Lin, M., Wang, X., Zhong, G., Yu, B., Hu, W., Dai, L., et al. (2015). Exon-intron circular RNAs regulate transcription in the nucleus. Nat Struct Mol Biol 22, 256–264.
Liu, H., Wang, X., Wang, H.D., Wu, J.J., Ren, J., Meng, L., Wu, Q., Dong, H., Wu, J., Kao, T.Y., et al. (2012). *Escherichia coli* noncoding RNAs can affect gene expression and physiology of *Caenorhabditis elegans*. Nat Commun 3, 1073.
Lopez Sanchez, M.I.G., Mercer, T.R., Davies, S.M.K., Shearwood, A.M.J., Nygård, K.K.A., Richman, T.R., Mattick, J.S., Rackham, O., and Filipovska, A. (2011). RNA processing in human mitochondria. Cell Cycle 10, 2904–2916.
Memczak, S., Jens, M., Elefsinioti, A., Torti, F., Krueger, J., Rybak, A., Maier, L., Mackowiak, S.D., Gregersen, L.H., Munschauer, M., et al. (2013). Circular RNAs are a large class of animal RNAs with regulatory potency. Nature 495, 333–338.
Mercer, T.R., Neph, S., Dinger, M.E., Crawford, J., Smith, M.A., Shearwood, A.M.J., Haugen, E., Bracken, C.P., Rackham, O., Stamatoyannopoulos, J.A., et al. (2011). The human mitochondrial transcriptome. Cell 146, 645–658.
Moore, S., Järvelin, A.I., Davis, I., Bond, G.L., and Castello, A. (2018). Expanding horizons: new roles for non-canonical RNA-binding proteins in cancer. Curr Opin Genets Dev 48, 112–120.
Moye-Rowley, W.S. (2003). Transcriptional control of multidrug resistance in the yeast Saccharomyces. Prog Nucleic Acid Res Mol Biol 73, 251–279.
Patop, I.L., Wüst, S., and Kadener, S. (2019). Past, present, and future of circRNA s. EMBO J 38, e100836.
Quirós, P.M., Langer, T., and López-Otín, C. (2015). New roles for mitochondrial proteases in health, ageing and disease. Nat Rev Mol Cell Biol 16, 345–359.
Salzman, J., Gawad, C., Wang, P.L., Lacayo, N., and Brown, P.O. (2012). Circular RNAs are the predominant transcript isoform from hundreds of human genes in diverse cell types. PLoS ONE 7, e30733.
Scheibye-Knudsen, M., Fang, E.F., Croteau, D.L., Wilson Iii, D.M., and Bohr, V.A. (2015). Protecting the mitochondrial powerhouse. Trends Cell Biol 25, 158–170.
Schmidt, O., Pfanner, N., and Meisinger, C. (2010). Mitochondrial protein import: from proteomics to functional mechanisms. Nat Rev Mol Cell Biol 11, 655–667.
Shan, G. (2010). RNA interference as a gene knockdown technique. Int J Biochem Cell Biol 42, 1243–1251.
Sheng, Z., Wang, X., Xu, G., Shan, G., and Chen, L. (2019). Analyses of a panel of transcripts identified from a small sample size and construction of RNA networks in hepatocellular carcinoma. Front Genet 10.
Shimada, E., Ahsan, F.M., Nili, M., Huang, D., Atamdede, S., TeSlaa, T., Case, D., Yu, X., Gregory, B.D., Perrin, B.J., et al. (2018). PNPase knockout results in mtDNA loss and an altered metabolic gene expression program. PLoS ONE 13, e0200925.
Smirnov, A., Comte, C., Mager-Heckel, A.M., Addis, V., Krasheninnikov, I.A., Martin, R.P., Entelis, N., and Tarassov, I. (2010). Mitochondrial enzyme rhodanese is essential for 5 S ribosomal RNA import into human mitochondria. J Biol Chem 285, 30792–30803.
Smith, A.C., and Robinson, A.J. (2015). MitoMiner v3.1, an update on the mitochondrial proteomics database. Nucleic Acids Res 44, D1258–D1261.
Sokol, A.M., Sztolsztener, M.E., Wasilewski, M., Heinz, E., and Chacinska, A. (2014). Mitochondrial protein translocases for survival and wellbeing. FEBS Lett 588, 2484–2495.
Sun, L., Fazal, F.M., Li, P., Broughton, J.P., Lee, B., Tang, L., Huang, W., Kool, E.T., Chang, H.Y., and Zhang, Q.C. (2019). RNA structure maps across mammalian cellular compartments. Nat Struct Mol Biol 26, 322–330.
Szabo, L., and Salzman, J. (2016). Detecting circular RNAs: bioinformatic and experimental challenges. Nat Rev Genet 17, 679–692.
Topf, U., Wrobel, L., and Chacinska, A. (2016). Chatty mitochondria: keeping balance in cellular protein homeostasis. Trends Cell Biol 26, 577–586.

Van Houten, B., Woshner, V., and Santos, J.H. (2006). Role of mitochondrial DNA in toxic responses to oxidative stress. DNA Repair 5, 145–152.
Venegas, V., and Halberg, M.C. (2012). Measurement of mitochondrial DNA copy number. In Mitochondrial Disorders (Springer), pp. 327–335.
Vyas, S., Zaganjor, E., and Haigis, M.C. (2016). Mitochondria and cancer. Cell 166, 555–566.
Walter, P., and Blobel, G. (1982). Signal recognition particle contains a 7S RNA essential for protein translocation across the endoplasmic reticulum. Nature 299, 691–698.
Wang, G., Chen, H.W., Oktay, Y., Zhang, J., Allen, E.L., Smith, G.M., Fan, K.C., Hong, J.S., French, S.W., McCaffery, J.M., et al. (2010). PNPASE regulates RNA import into mitochondria. Cell 142, 456–467.
Wang, X., and Shan, G. (2018). Nonradioactive Northern blot of circRNAs. In Circular RNAs (Springer), pp. 135–141.
Weidberg, H., and Amon, A. (2018). MitoCPR—A surveillance pathway that protects mitochondria in response to protein import stress. Science 360, eaan4146.
Weir, H.J., Yao, P., Huynh, F.K., Escoubas, C.C., Goncalves, R.L., Burkewitz, K., Laboy, R., Hirschey, M.D., and Mair, W.B. (2017). Dietary restriction and AMPK increase lifespan via mitochondrial network and peroxisome remodeling. Cell Metab 26, 884–896.e5.
Wesselhoeft, R.A., Kowalski, P.S., and Anderson, D.G. (2018). Engineering circular RNA for potent and stable translation in eukaryotic cells. Nat Commun 9, 2629.
Wieckowski, M.R., Giorgi, C., Lebiedzinska, M., Duszynski, J., and Pinton, P. (2009). Isolation of mitochondria-associated membranes and mitochondria from animal tissues and cells. Nat Protoc 4, 1582–1590.
Wiedemann, N., and Pfanner, N. (2017). Mitochondrial machineries for protein import and assembly. Annu Rev Biochem 86, 685–714.
Williamson, C.D., Wong, D.S., Bozidis, P., Zhang, A., and Colberg-Poley, A.M. (2015). Isolation of endoplasmic reticulum, mitochondria, and mitochondria-associated membrane and detergent resistant membrane fractions from transfected cells and from human cytomegalovirus-infected primary fibroblasts. Curr Protocols Cell Biol 68, 3–27.
Wrobel, L., Topf, U., Bragoszewski, P., Wiese, S., Sztolsztener, M.E., Oeljeklaus, S., Varabyova, A., Lirski, M., Chroscicki, P., Mroczek, S., et al. (2015). Mistargeted mitochondrial proteins activate a proteostatic response in the cytosol. Nature 524, 485–488.
Young, J.C., Hoogenraad, N.J., and Hartl, F.U. (2003). Molecular chaperones Hsp90 and Hsp70 deliver preproteins to the mitochondrial import receptor Tom70. Cell 112, 41–50.
Zhang, X., Zuo, X., Yang, B., Li, Z., Xue, Y., Zhou, Y., Huang, J., Zhao, X., Zhou, J., Yan, Y., et al. (2014). MicroRNA directly enhances mitochondrial translation during muscle differentiation. Cell 158, 607–619.
Zong, W.X., Rabinowitz, J.D., and White, E. (2016). Mitochondria and cancer. Mol Cell 61, 667–676.
Zou, Y., Liu, Y., Wu, X., and Shell, S.M. (2006). Functions of human replication protein A (RPA): from DNA replication to DNA damage and stress responses. J Cell Physiol 208, 267–273.

SUPPORTING INFORMATION

Figure S1 Features of mecciRNAs, related to Figure 1.

Figure S2 Experimental verification of mecciRNAs, related to Figure 1.

Figure S3 Analyses of related NGS data, related to Figure 1.

Figure S4 Mitochondrial and cytosolic distributions of mecciRNAs, related to Figure 1.

Figure S5 mecciND1 interacts with RPA70 and RPA32, related to Figure 2.

Figure S6 mecciND5 interacts with hnRNPA proteins, related to Figure 2.

Figure S7 Correlations between mecciND1 and mitochondrial RPA levels, related to Figure 3.

Figure S8 Correlations between mecciND5 and mitochondrial hnRNPA levels, related to Figure 4.

Figure S9 mecciND1 and mecciND5 copy number per cell and i*n vitro* assays, related to Figure 5.

Figure S10 Western blots of proteins in the RNA-IP (for Figure 7A) and knockdown and overexpression of PNPASE, related to Figure 5.

Figure S11 Secondary structure of mecciND1 and mecciND5, related to Figure 5.

Figure S12 mecciND1 levels under stress, mecciND5 levels in HCC, mecciRNAs in *S. pombe* and *C. elegans*. Related to Figure 6.

Table S1 List of mecciRNAs from RNA-seq data

Table S2 Mass spectrometry results of mecciND1 and mecciND1 pull-down proteins

Table S3 Oligos used in this study

The supporting information is available online at http://life.scichina.com and https://link.springer.com. The supporting materials are published as submitted, without typesetting or editing. The responsibility for scientific accuracy and content remains entirely with the authors.